University of Alberta

Patient positioning accuracy and dose delivery assessment on a TomoTherapy Hi-Art II system unit

by

Donata Monika Drabik

A thesis submitted to the Faculty of Graduate Studies and Research
in partial fulfillment of the requirements for the degree of

Master of Science
in
Medical Physics

Department of Physics

Edmonton, Alberta
Fall , 2007

Library and Archives Canada

Published Heritage Branch

395 Wellington Street
Ottawa ON K1A 0N4
Canada

Bibliothèque et Archives Canada

Direction du Patrimoine de l'édition

395, rue Wellington
Ottawa ON K1A 0N4
Canada

Your file Votre référence
ISBN: 978-0-494-33234-4
Our file Notre référence
ISBN: 978-0-494-33234-4

NOTICE:
The author has granted a non-exclusive license allowing Library and Archives Canada to reproduce, publish, archive, preserve, conserve, communicate to the public by telecommunication or on the Internet, loan, distribute and sell theses worldwide, for commercial or non-commercial purposes, in microform, paper, electronic and/or any other formats.

The author retains copyright ownership and moral rights in this thesis. Neither the thesis nor substantial extracts from it may be printed or otherwise reproduced without the author's permission.

AVIS:
L'auteur a accordé une licence non exclusive permettant à la Bibliothèque et Archives Canada de reproduire, publier, archiver, sauvegarder, conserver, transmettre au public par télécommunication ou par l'Internet, prêter, distribuer et vendre des thèses partout dans le monde, à des fins commerciales ou autres, sur support microforme, papier, électronique et/ou autres formats.

L'auteur conserve la propriété du droit d'auteur et des droits moraux qui protège cette thèse. Ni la thèse ni des extraits substantiels de celle-ci ne doivent être imprimés ou autrement reproduits sans son autorisation.

In compliance with the Canadian Privacy Act some supporting forms may have been removed from this thesis.

While these forms may be included in the document page count, their removal does not represent any loss of content from the thesis.

Conformément à la loi canadienne sur la protection de la vie privée, quelques formulaires secondaires ont été enlevés de cette thèse.

Bien que ces formulaires aient inclus dans la pagination, il n'y aura aucun contenu manquant.

Canada

Abstract

The first part of this thesis describes a technique that can be implemented in-house in order to evaluate the efficacy of immobilization and image guided setup of patients with different treatment sites on helical tomotherapy (HT). This technique uses an analysis of alignment shifts between kVCT and post MVCT images. The determination of those shifts is used to define appropriate PTV internal margins. Since shrinkage in H&N patients appears during the course of treatment and is observed to influence immobilization accuracy, the second project is designed to evaluate the impact of anatomy changes on dose delivery to the volumes of interest (VOIs). Anatomy changes are sometimes a cause of overdosage of organs at risk (OARs) as well as increases in inhomogeneity within the target volumes. The study implies that adaptive planning should be introduced to the treatment course if the OAR sparing is meant to be at least maintained.

Acknowledgments

I would like to thank my wonderful friends, especially Tara & Alasdair, Andrée & Matt, Dave, Lesley, Colleen and Rehana for their friendship and support in both the good times and bad times over the course of my studies.

I also want to say thank you to Dr. Marc MacKenzie who is a great person and a great supervisor and Dr. Gino Fallone for all his support which helped me graduate and find a job that I wanted.

It was a pleasure to work with the staff and students in Department of Medical Physics at the Cross Cancer Institute.

And finally, special thanks to my loving family.

Sincerely yours,

Donata Drabik

Table of contents

Chapter 1. Introduction 1

1. Radiation therapy (RT) 1

1.1 Three dimensional conformal radiotherapy (3D CRT) 1

1.2 Intensity Modulated Radiotherapy (IMRT) 1

1.3 Image guided radiotherapy (IGRT) 2

1.4 Adaptive radiotherapy (ART) 3

2. Introduction to Helical TomoTherapy 3

2.1 Imaging - kilo Voltage Computed Tomography (kVCT) – CT Simulation 5

2.1.1 Terms and Concepts for Volumes and Margins 6

2.2 Treatment planning 7

2.3 Mega Voltage Computed Tomography (MVCT) – positioning verification 10

2.4 Image registration 11

2.4.1 Patient Positioning & Immobilization 13

2.5 Radiation treatment on HT 14

2.6 Treatment verification 14

3. Clinical Outcome for Head and Neck Cancer Treatment 15

3.1 Head and Neck Cancer Specification 15

3.2 Problems in radiation delivery to head and neck tumour 15

4. Thesis objectives 19

Bibliography 20

Chapter 2. Quantifying appropriate PTV setup margins: analysis of patient setup fidelity and intrafraction motion using post treatment

megavoltage CT (MVCT) scans 28

1. Introduction 28

2. Methods and Materials 30

3. Results 32

3.1. Statistics for translations from manual and automatic registration 32

3.1.1 Automatic registration 32

3.1.2 Manual registration by physicist 33

3.2. Analysis of translations expressed as net radial shift 33

3.2.1. Automatic registration 33

3.2.2. Manual registration by physicist 34

4. Discussion 37

4.1 Translations from manual and automatic registration 37

4.1.1 Prostate 37

4.1.2 Glioblastoma multiforme 37

4.1.3 Head and neck 38

4.1.4 Automatic and manual data for all sites 38

4.2 Translations expressed as net radial shift 39

4.3 Limitations 40

5 Conclusion 40

Bibliography 42

Chapter 3. Dose Delivery Assessment for Head and Neck Cancers Using *Planned Adaptive* Helical TomoTherapy Software 45

1. Introduction 45

2. Methods and Materials 48

3. Results 51

3.1. Volume analysis 51

3.2. Dosimetric analysis 67

4. Discussion 71

5. Conclusion 74

Bibliography 76

Chapter 4. Summary 79

List of tables

Table 2-1.	Automatic registration data, N – number of post treatment images	34
Table 2-2.	Manual registration data, N – number of post treatment images	34
Table 2-3.	Radii obtained from automatic and manual datasets, N – number of post treatment images	34
Table 3-1.	H&N treatment protocol dose constraint analysis	48
Table 3-2.	Linear regression results of VOIs for Patient 1	52
Table 3-3.	Linear regression results of VOIs for Patient 2	55
Table 3-4.	Linear regression results of VOIs for Patient 3	58
Table 3-5.	Linear regression results of VOIs for Patient 4	61
Table 3-6.	Linear regression results of VOIs for Patient 5	64
Table 3-7.	Percentage volume changes per fraction for all patients	67
Table 3-8.	Percentage dose difference between delivered and planned treatment for Patient 1	68
Table 3-9.	Percentage dose difference between delivered and planned treatment for Patient 2	69
Table 3-10.	Percentage dose difference between delivered and planned treatment for Patient 3	69
Table 3-11.	Percentage dose difference between delivered and planned treatment for Patient 4	70
Table 3-12.	Percentage dose difference between delivered and planned treatment for Patient 5	71

List of figures

Figure 1-1.	Schematic illustration of multileaf collimator set to the tumour shape, arrows and dashed lines represent radiation beam	2
Figure 1-2.	HT processes scheme - adaptive radiotherapy currently available at the CCI	5
Figure 1-3.	An example of planning sinogram for a H&N patient on Tomotherapy. The grey scale intensity is directly related to the planned energy fluence for each leaf (along matrix row) and gantry rotation angle (along matrix column). This example shows a total of 19 complete continuous gantry rotations (360° each).	10
Figure 2-1.	Coordinate system on HT unit	30
Figure 2-2.	Displayed images; a) top left – MVCT image, b) bottom left – kVCT image, c) right – registration of both images, checker example shown in yellow	31
Figure 2-3.	Average X, Y and Z shifts for prostate sites	35
Figure 2-4.	Average X, Y and Z shifts for GBM sites	35
Figure 2-5.	Average X, Y and Z shifts for H&N sites	36
Figure 2-6.	Average and median values of radius for prostate, GBM and H&N sites	36
Figure 3-1.	Linear regression for the PTV 60, Patient 1	53
Figure 3-2.	Linear regression for the PTV 54, Patient 1	53
Figure 3-3.	Linear regression for the volume of left parotid, Patient 1	54

Figure 3-4.	Linear regression for the volume of right parotid, Patient 1	54
Figure 3-5.	Linear regression results for PTV60 for Patient 2	56
Figure 3-6.	Linear regression results of the PTV54 for Patient 2	56
Figure 3-7.	Linear regression results of the volume of left parotid for Patient 2	57
Figure 3-8.	Linear regression results of the volume of right parotid for Patient 2	57
Figure 3-9.	Linear regression results of the PTV60 for Patient 3	59
Figure 3-10.	Linear regression results of the PTV54 for Patient 3	59
Figure 3-11.	Linear regression results of the volume of left parotid for Patient 3	60
Figure 3-12.	Linear regression results of the volume of right parotid for Patient 3	60
Figure 3-13.	Linear regression results of the PTV60 for Patient 4	61
Figure 3-14.	Linear regression results of the PTV54 for Patient 4	62
Figure 3-15.	Linear regression results of the volume of left parotid for Patient 4	62
Figure 3-16.	Linear regression results of the volume of right parotid for Patient 4	63
Figure 3-17.	Linear regression results of the PTV60 for Patient 5	64
Figure 3-18.	Linear regression results of the PTV54 for Patient 5	65
Figure 3-19.	Linear regression results of the volume of left parotid for Patient 5	65
Figure 3-20.	Linear regression results of the volume of right parotid for Patient 5	66

List of abbreviations

3D CRT	*Thee Dimensional Conformal Radiation Therapy*
ART	*Adaptive Radiation Therapy*
CCI	*Cross Cancer Institute*
CT	*Computed Tomography*
CTV	*Clinical Target Volume*
DQA	*Delivery Quality Assurance*
DVH	*Dose Volume Histogram*
EFF	*Extracted feature fusion*
GBM	*Glioblastoma Multiformae*
GTV	*Gross Tumour Volume*
H&N	*Head and Neck*
HT	*Helical Tomotherapy*
IGAR	*Image guided adaptive radiotherapy*
IGRT	*Image Guided Radiation Therapy*
IMRT	*Intensity Modulated Radiation Therapy*
kVCT	*kilo Voltage Computed Tomography*
linac	*Medical linear accelerator*
MI	*Mutual Information*
MLC	*Multileaf Collimator*
MVCT	*Mega Voltage Computed Tomography*
NTCP	*Normal Tissue Complication Probability*

OAR	*Organ at Risk*
PTV	*Planned Target Volume*
PTV 60	*Planned Target Volume with contours defined by 60 Gy isodose line*
PTV 54	*Planned Target Volume with contours defined by 54 Gy isodose line*
ROI	*Region of Interest*
RT	*Radiation Therapy*
TCP	*Tumour control probability*
TERMA	*Total Energy Release per unit Mass*
VOI	*Volume of Interest*

Chapter 1. Introduction

1. Radiation therapy (RT)

About half of all cancer patients receive radiotherapy [Corbett et al., 1992]. The process of treatment delivery is researched in order to obtain more time efficient and effective treatment. Some of the modern techniques of radiation treatment are as described below.

1.1. Three dimensional conformal radiotherapy (3D CRT)

Three dimensional conformal radiotherapy (3D CRT) designs treatments that are based on 3D anatomic information of the patient and deliver dose distributions that conform adequately to the target volume [Khan, 2003]. Some of the goals of 3D CRT are: (i) delivery of high dose to a precisely localized volume that closely conforms to the shape of the tumour volume to maximize tumour control probability (TCP); and (ii) minimization of the dose to the neighboring sensitive structures. 3D CRT is characterized by high gradient regions surrounding the tumour in order to minimize normal tissue complication probability (NTCP). The achievement of those goals is feasible when the treatment plan delivers the dose accurately to the geometric position of the tumour [Hamilton et al., 2005].

1.2. Intensity Modulated Radiotherapy (IMRT)

Intensity Modulated Radiotherapy (IMRT) is a modality in which incident radiation beam is purposely modulated in order to improve the dose distribution in the patient produced by many fields. Treatment with this technique is enabled via availability of multileaf collimator (MLC) in the modern treatment machines and utility of optimization algorithms.

Optimization algorithms calculate optimal dose distributions using set of constraints. The presence of optimized dose distribution and the associated high dose

gradients for the individual patient anatomy impose the requirement of accurate patient positioning [Lia et al., 2000]. In a fractionated radiation treatment course it is critical to account for day-to-day patient misalignments and changes in the internal anatomy or risk an underdosage of the target or overdosage of the nearby organ at risk (OAR).

Intensity modulation of the beam can be achieved using a beam defining device known as an MLC that has usually about 50 to 120 movable tungsten leaves which are thick along the incident beam direction, but narrow, with a typical size of 5 or 10 mm, to allow for fine shaping of arbitrary beam apertures (Figure 1-1) [Fiveash et al., 2002]. These MLC leaves are arranged in pairs and their positioning with respect to beam on time is controlled by a computer. The appropriate arrangement of the leaves enables the shaping of the radiation beam to the tumour volume.

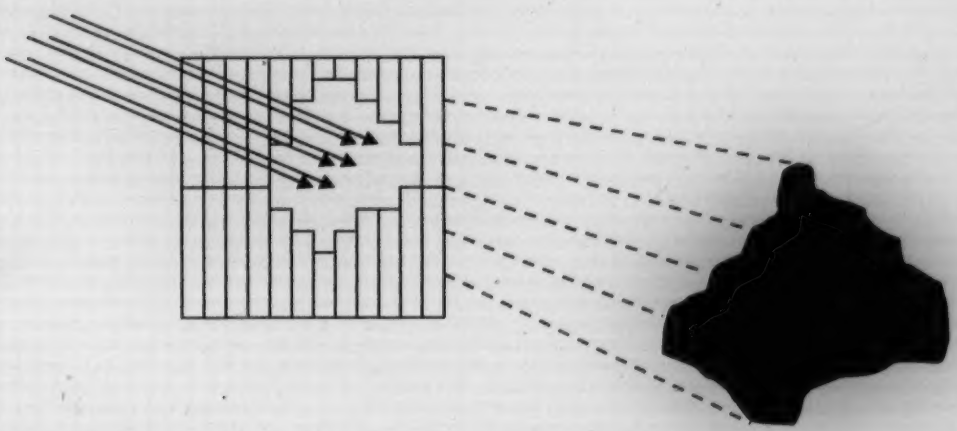

Figure 1-1. Schematic illustration of a multileaf collimator set to the tumour shape, arrows and dashed lines represent radiation beam.

1.3. Image guided radiotherapy (IGRT)

Image guided radiotherapy (IGRT) is an emerging option for patient setup, and is especially useful in the more advanced forms of radiation delivery such as intensity modulated radiation therapy where high dose gradients and conformal avoidance make patients positioning especially critical. IGRT uses three dimensional images that give precise information about patient position [Jaffray et al., 2002; Ruchala et al., 2002; Yan

et al., 1997]. The localization of the targets and conformal avoidance of sensitive structures is achieved using on-line 3D imaging at each treatment fraction. It is generally known that IGRT gives the possibility to reduce planning target volume (PTV) margins and delivers a higher dose to the target while, at the same time, sparing OARs. The rigid body registration of the daily patient image to the planning image focusing on the bony anatomy or a soft tissue is most commonly used in IGRT in order to quantify patient/organ geometric variations. A rigid body motion assumes no shape change in the organ [Yan et al., 2005]

1.4. Adaptive radiotherapy (ART)

Adaptive radiotherapy (ART) is a novel approach that offers the techniques to deal with the problem of changing treatment conditions (e.g. patient weight loss, shrinking tumours, and mobile tumours). It involves incorporation of the feedback from the treatment results to the image-guided radiotherapy processes [Mackie et al., 2003]. It can be defined as a procedure of adjustment of the treatment to the variations of patient anatomy during the course of treatment in order to maintain or improve the accuracy of dose delivery and level of OAR sparing. It usually involves re-planning and modification of dose delivery as well as some other treatment conditions (such as change of immobilization device). ART was introduced into the radiotherapy process fairly recently and is not commonly used yet. It was designed to re-optimize the treatment plan and dose delivery of the individual patient in order to minimize the detrimental effects of treatment variation on the individual patient [Yan et al., 1998].

2. Introduction to Helical Tomotherapy

A technique, once considered novel but which is becoming increasingly common, for delivery of radiation therapy is offered by helical tomotherapy (HT). HT is a combination of 6 MV linac and helical CT scanner [Mackie, 2006]. The radiation is delivered continuously in a helical manner while the patient placed on the couch is driven into the gantry. The beam is collimated using binary MLC that consists of 64 leaves, each

projecting a width of 6.25 mm at isocentre. The leaves can rapidly change their position between the open (leaf retracted) and closed (leaf blocking) states during treatment to modulate the beam. The total fan beam width at isocentre is 40 cm. HT not only delivers highly conformal IMRT, but also has the ability to perform a megavoltage computed tomography (MVCT) utilizing a 3.5 MV photon beam. HT Hi-Art system contains an arc-shaped array of 738 xenon detectors that was originally designed for the General Electric Computed Tomography scanner (GE CT) [Keller et al., 2002; Mackie et al., 2003; Ruchala et al., 1999]. Source to detector distance is 145 cm whereas source to isocentre is 85 cm. MLC of HT scanner has the field of view that enables to use only 540 detectors in imaging, the remaining ones are unused [Meeks et al., 2005].

In addition, software resident on the HT unit calculates the positioning shifts between the MVCT image and the planning data, to which patients are repositioned [Langen et al., 2005; Mackie et al., 2003]. HT also gives a possibility of radiation delivery assessment which is further explained in Chapter 3 of this thesis; this opens the possibility of improvement of the delivery by modification/re-optimization of the treatment plan [Beavis, 2004; Langen et al., 2005; Mackie et al., 2003].

Since HT Hi-Art II unit is an integrated system of several devices it is nearly self sufficient in terms of the radiotherapy process. The unit has a treatment planning component, MV imaging, delivery quality assurance (DQA) tools, and software that enables assessment of dose delivery. A current scheme of HT process is presented below.

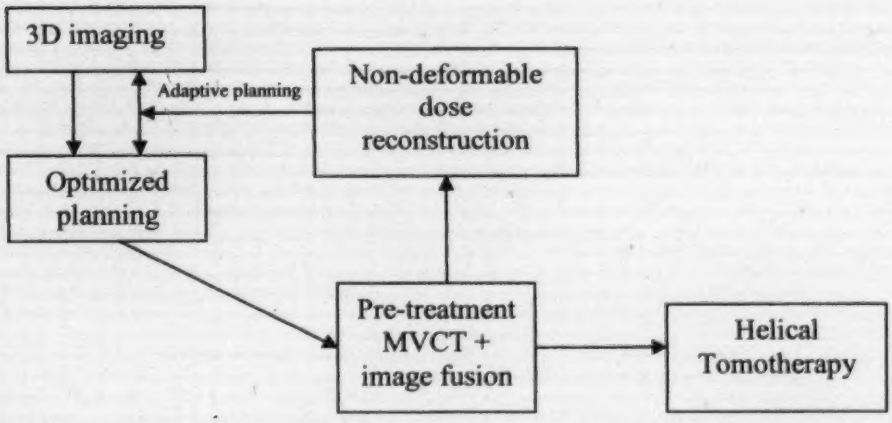

Figure 1-2. HT processes scheme - adaptive radiotherapy currently available at the Cross Cancer Institute (CCI)

2.1. Imaging - kilo Voltage Computed Tomography (kVCT) – CT simulation

The radiotherapy process begins with the diagnosis and the decision to treat patient via radiation therapy. Subsequently, a three dimensional image is acquired for treatment planning. The imaging technique that is the most commonly used for treatment planning, as well as for HT treatment planning, is kilo voltage Computed Tomography (kVCT).

Generally, a kVCT scanner is equipped with an x-ray tube and a detector array, the latter being located on the opposite side of a ring gantry from the x-ray tube tube on. The ring gantry rotates around the patient delivering a beam of x-rays and the detectors measure the intensity of X-ray radiation that is transmitted through the patient's body. The kVCT images are reconstructed most commonly using the filtered backprojection method, where the projection data acquired during the scan are directly related to the Fourier transform of the object being imaged via the central slice theorem [Bracewell, 1986]. The main reason kVCT images are used in treatment planning is the fact that each pixel value of the image corresponds to the Hounsfield unit, which depends on the attenuation coefficient of the anatomical structure that was imaged. Because dose deposition depends on the attenuation properties of the tissues and energy of the radiation

beam used for imaging, the dose distribution in the patient for the treatment plan can be calculated.

The kVCT images have acceptable soft tissue contrast with high resolution defined as a 512 x 512 matrix, with a field of view equal to 40 cm and a pixel size of 0.78 mm [Viswanathan et al., 2007; Voroney et al., 2006]. Therefore the kVCT images enable identification of the volumes of interest (VOIs) and contouring that is necessary in the modern treatment planning techniques.

2.1.1. Terms and Concepts for Volumes and Margins

Current treatment planning methods assume static targets and static structures. Positioning uncertainties are accounted for by adding treatment margins around the structures. A margin represents a ''hard boundary'' which a particular isodose line should enclose or avoid [Lia et al., 2000]. To maximize the tumor control and minimize the complication in surrounding tissues, the appropriate definition and choice of gross tumor volume (GTV), clinical target volume (CTV) and planned target volume (PTV) has to be done [Antolak et al., 1999; Hamilton et al,. 2005; ICRU 50; Mackie et al., 2003; Prisciandaro et al., 2004]. The definitions of the first two volumes are as follows: *"GTV is the gross palpable or visible/demonstrable extent and location of malignant growth"* [ICRU 50, Van Dyk, 1999], whereas *"CTV is a tissue volume that contains demonstrable GTV and/or subclinical microscopic malignant disease, which has to be eliminated. This volume thus has to be treated adequately in order to achieve the aim of therapy, cure or palliation"* [ICRU 50].While the GTV and CTV will, ideally, be well defined, PTV is the volume which is based on a geometrical concept and is used for treatment planning [ICRU suppl. 62]. PTV is defined as the volume "*taking into consideration the net effect of all the possible geometrical variations, in order to ensure that the prescribed dose is actually absorbed in the CTV*" [ICRU 50]. The appropriate choice of margins is very important. If the margins on the target volumes are chosen incorrectly the creation of successful treatment plan is impossible, especially in a modality that creates steep gradients of dose. If the tumor does not get all absorbed dose that is prescribed, some of the cancer cells may survive and the disease may recur. It is because of this that the

internal position of the tumor must be known before each treatment as well as positioning accuracy and fidelity. For example, displacement of the organ such as prostate is either monitored just before radiation treatment or a larger PTV is implemented to account for every possible position of the target. On the other hand, caution must be taken to spare a normal tissue as much as possible, especially if the tumor is surrounded by critical structures. The greater the irradiation of critical structures, the more normal tissue complications may be expected.

One way to achieve either greater sparing or dose escalation with equal dose to the critical structure is to reduce the margins required on the PTV [Mackie et al., 2003]. This is not an simple goal to achieve since many factors account for the choice of margin such as intra- and interfraction motion of organs and patient setup variability [Antolak et al., 1998; Huntzinger et al., 2006; Stroom et al., 2000].

The margins of treatment volumes must be designed to account for treatment errors as mentioned above. In general, the errors can be divided into two groups: systematic and random errors. Systematic errors arise mostly in the preparation stage of the treatment whereas random errors occur during the execution of the treatment. While it is impossible to eliminate all these errors, an understanding of the source and magnitude of these errors as well as its minimization techniques is important for the success of radiation treatment [Hanley et al., 1997; Hoogeman et al., 2005].

2.2. Treatment planning

In general, the planning of a course of radiation therapy treatment for cure or symptomatic control of a tumour must be performed before a patient can be treated. The planning is designed to achieve the prescription radiation dose by accounting for machine dose delivery capabilities and accessories if they are required.

Forward planning was the traditional method used to plan treatments delivered by machines not capable of the most modern radiotherapy techniques, such as IMRT. When forward planning was performed the parameters of the treatment were set and, using the dose calculation algorithm, the dose distribution in the patient was calculated and

evaluated. A decision was made whether or not the plan needed modifications based on how well it achieved the objectives of target coverage and critical structure sparing.

Inverse planning is a modern treatment planning technique that is used along with the modern techniques of radiation treatment such as IMRT or HT. The idea of inverse planning is to define dose objectives and constrains to the target and OARs, and then use iterative optimization techniques with the dose calculation algorithm to design the treatment delivery.

HT treatment planning can be started once HT treatment planning station receives kVCT images having all regions of interest (ROIs) contoured already. The inverse treatment planning parameters such as prescription dose to the PTV, tolerance doses to the ROIs, field width that is defined as the thickness of the treatment field at the machine isocenter, pitch, that describes the amount of beam overlap that occurs for each gantry rotation (lower values imply more overlap), dose calculation grid that specifies the image resolution for the transverse plane (this resolution is used for dose calculation) and optimization mode are introduced to the optimizer.

In general, *"the ideal optimization technique should be robust, flexible and fast. The algorithm should also minimize the memory demands, and it should reach an optimal solution in a limited number of iterations"* [Van Dyk, 1999].

HT uses the convolution / superposition algorithm for dose calculations. First, the incident energy fluence modified by MLC in the patient is modeled. The transport of charged particles and photon scatter is modeled by kernels that are pre-calculated using Monte Carlo method [Mackie et al., 2003]. Initial beam weights are computed and the full dose distribution is calculated by the optimizer. Each beamlet represents the beam that is shaped by MLC at given projection angle. A comparison between desired and obtained dose distribution is then made. As a consequence the update weight for each pencil beam is determined. The new pencil beam weights are used to recalculate dose distribution. This process is repeated until satisfactory dose distribution in the patient is obtained which is assessed using the dose volume histogram (DVH) for each contoured target volume and OAR.

Also, the user has a possibility to chose the optimization mode out of three options: (i) Total Energy Released per Unit Mass (TERMA), that is the fastest and least

accurate, based only on primary beam attenuation using the energy absorption coefficients, (ii) Full Scatter, that calculates dose distributions for each iteration to optimize the treatment plan; these iterations require a few minutes to calculate, (iii) beamlet, the most commonly used, that pre-computes the dose distributions for possible leaf openings; the pre-computation requires several hours but after that each iteration calculates within seconds.

DVH analysis enables quantitative evaluation of the three dimensional dose distribution for a given ROI in a simpler format. It is the binning of the three dimensional dose volume elements (voxels) into dose bins, and presented in the differential (direct) or integral (cumulative) form, and relative to absolute or relative volumes (normalized to each ROIs volume). In general, DVH is a function described in two dimensional array, where X axis describes the dose values and Y axis gives the absolute or percentage volume of given ROI. The loss of spatial relationship to the ROI is a serious limitation of presenting data in the form of DVH, but it is nevertheless commonly used [Schell et al., 1991; Seargo et al., 1992]. As a result of the optimizer calculations, a planning sinogram is generated. It is a two dimensional array that contains the planned energy fluence that is the result of the optimization process (Figure 1-3). The rows correspond to the projection numbers (and hence bear a relationship to treatment time) and the columns are the MLC leaf numbers (from one to sixty four). The values in the array represent radiation intensity. Once the treatment plan is calculated and deemed acceptable in terms of treatment goals, the planned data are verified by a series of measurements defined in DQA procedure. The treatment plan of the patient is transferred to a phantom made of radiologically water equivalent plastic, the so called 'Cheese' phantom, and re-calculated. A radiograph film and an ion chamber is inserted into the phantom and delivered dose is measured for the purpose of comparing the re-calculated (phantom) and measured dose. When the comparison is found to be satisfactory (e.g. within 3% of the planning dose in the high dose regions), the patient treatment is allowed to proceed [Mackie et al., 2003].

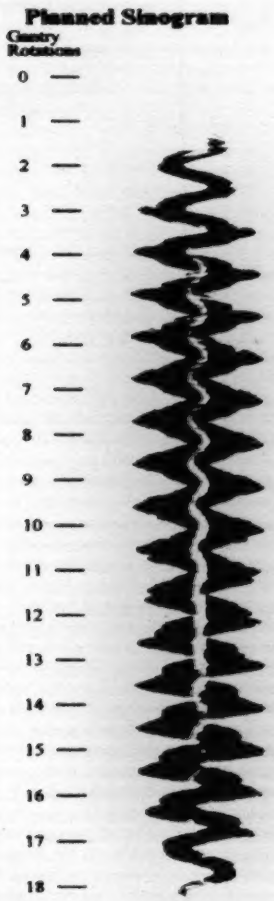

Figure 1-3. An example of planning sinogram for a H&N patient on Tomotherapy. The grey scale intensity is directly related to the planned energy fluence for each leaf (along matrix row) and gantry rotation angle (along matrix column). This example shows a total of 19 complete continuous gantry rotations (360° each).

2.3. Mega Voltage Computed Tomography (MVCT) – positioning verification

HT delivers IGRT and is capable of MVCT imaging. A pre-treatment CT scan is performed for the verification of the patient position and the location of the internal anatomy. This allows for any relocation of the patient that might be necessary to ensure dose delivery to the right tissues within the patient. In addition, scan can be performed with a fine, normal or coarse scan setting that corresponds to a reconstructed slice spacing

of 2.5, 4 and 6 mm in the chosen area of patient anatomy; the jaw setting is fixed and a pitch of 1, 1.6 or 2.4 is used for these three scan settings.

MVCT can be also used for verification of the patient position after the treatment. Post treatment imaging technique and its application is further discussed in the subsequent sections of this thesis.

It is commonly known that MVCT images have inferior quality to kVCT. Generally, it is also known that the contrast and resolution of the CT images are related to each other. Greater inherent object contrast is required to see smaller objects. For high contrast objects such as air cavity in the plastic phantom, HT Hi-Art II system has a resolution limit of 1 - 1.2 mm that corresponds to the visibility of detailed shape of bone and distinction of sinuses and lungs. Also, an object that has the size of 2.5 cm can be seen on the MVCT images when its density difference from background is as small as 2 or 3%. This implies that density differences of 3 to 7% between anatomic structures made of soft tissue will generally not be well visible [Mackie, 2003]

In addition, the attenuation of the megavoltage beam is linear since, in this energy range, Compton interactions are dominant. As a result, the MVCT image pixel values correspond to the electron density of the anatomic structures being imaged [Van Dyk, 1999; Meeks et al., 2005].

2.4. Image registration

As previously mentioned in section 1.3, IGRT is commonly used for patient positioning purposes. Image registration methods are used to localize the target volume and reproduce accurately patient position before each fraction. There are two techniques of image registration: deformable (non-rigid) and non-deformable (rigid).

Rigid body registration is the most common technique used in IGRT. The assumption of a rigid body certainly simplifies the registration process. However, the techniques that use it have limited applicability. This is because many organs deform during the course of treatment [Barker et al., 2004; Gao et al., 2006; Rosu et. al, 2007]. In case of head anatomy it can be assumed that it is reasonably non-deformable, in regions such as the skull. Regions that change substantially between image acquisitions can bias

the result of rigid body registration and lead to significant errors. The algorithms used in rigid body image registration usually use points, surfaces or crest lines that are identified using differential geometric operators [Hill et al., 2001].

In Hi-Art Tomotherapy, the image registration is performed between the reconstructed kVCT - MVCT images to determine the patient position on the treatment couch. The planned treatment position is determined when the patient undergoes virtual simulation (acquisition of the planning kVCT image) prior to the start of treatment planning. Registration on HT is done using standard patient localization devices as well as fiducial markers during the simulation and each fraction of the treatment and utilizes both the kVCT and MVCT image. The automatic registration is done using Mutual Information (MI) algorithm called the full image technique or alternatively extracted feature fusion (EFF), where the registration parameters are determined by optimization of a similarity measure that depends on voxels in the reconstructed floating image with values typical for bone (above 1.1 g/cm3) or bone and tissue (above 0.3g/cm3). In other words, the following techniques are available in the software (i) bone technique, that uses only bone (high density) data points from both images; (ii) bone and tissue technique, that uses bone and tissue (high and low density) data points; and (iii) full image technique, that uses bone, tissue, and air data points from the images.

In addition, technique called "limited field of view" is available in order to have an option to discard artifact-distorted pixel values in the periphery of MVCT images that have smaller fields of view than the planning kVCT image.

Moreover, user of the operator station has several options to perform registration. There are three choices for the resolution (standard, fine and super fine) with which the images can be aligned and they vary among each other by the number of data points that are used to register. Also, depending on the site being treated, the operator can choose the structures (Hounsfield unit range) with respect to which registration is going to be made.

The results of automatic registration are typically readjusted by the operator who can manually alter the registration of the MVCT image with respect to the kVCT image using translational and rotational buttons [Boswell et al., 2006; Ruchala et al., 2002]. Once the registration is finalized, the software displays the translations (X, Y, Z) or

translations and rotations (X, Y, Z, pitch, roll and yaw). Based on the accepted registration, patient position can be manually or automatically adjusted.

However, the registration capabilities of HT can be also used for purposes other than patient positioning. The post treatment scanning can be used for net intrafraction motion assessment and quantification of the PTV margins as it is presented in Chapter 2.

Unfortunately HT has no capability of real time image registration / movement tracking so only the start (pre treatment MVCT) and end position (post treatment MVCT) of the patient/tumour can be investigated. However, taking into consideration the prostate localization study performed by Willoughby et al. [Willoughby et al., 2006], the majority of patients exhibit stable intrafraction prostate position, so that according to this observation, the measurement of the start and end position (net displacement), can be considered to be sufficient for PTV determination.

Non-rigid image registration uses algorithms that account for anatomical changes and may enable automatic re-contouring of targets and organs at risk, which is extremely useful for dose recalculation purposes. The technique is designed to track given voxels of tissue throughout the course of treatment and accumulate its dose. However, non-rigid registration is not sufficiently advanced to be used routinely, and will thus not be discussed further [Lu et al., 2006, Mackie et al., 2003; Pekar et al., 2006].

2.4.1. Patient Positioning & Immobilization

The problem of underdosage of a treated region or overdosage of normal tissues is more complicated than just appropriate treatment volume margin definition. It can also occur due to inappropriate patient positioning on the treatment couch. The goal of using patient positioning and immobilization devices is to fix the relationship between radiation beam and the target as well as maintain the position during each treatment. Skin marks are frequently used on patients for setup purposes. Furthermore, the treatment of specific sites involves particular immobilization techniques [Creutzberg et al., 1992; Delannes et al., 1991; Dietmar et al., 2006; Sharp et al., 2005; Van Dyk, 1999; Zierhut et al., 1994]. For example, in our centre the prostate cases often have "modest" immobilization, which means that ankle and/or knee rests are used only. The most common immobilization

device for head and neck (H&N) cancer patients and central nervous system cancer patients, such as glioblastoma multiformae (GBM), is a base plate with a facial fixation mask with the setup marks on the mask [Van Dyk, 1999]. On the other hand, it should be noted that even with a good immobilization device, weight loss and tumour shrinkage in patients, which can depend on the time elapsed since the first fraction was delivered, can influence the efficacy of any immobilization device.

2.5. Radiation Treatment on HT

In order to use HT 'in the clinic', daily quality assurance of dose delivery has to be performed each morning before machine is used for treatment purposes. Secondly, when the patient is to be treated the appropriate positioning has to be assured and fiducial marks are made before delivery of the first fraction and used before each subsequent fraction for initial setup. Once the patient is set on the couch with all appropriate positioning and immobilization devices, an MVCT image is acquired and registered with the planning kVCT in order to verify and adjust, if required, the patient/target setup. The setup correction technique that is currently used involves application of the couch shifts in the given directions as required. Finally, the treatment is delivered to the patient. During this step, the synchronization and control of the gantry, MLC and couch is managed by the delivery computer according to the optimized treatment plan. Each device and process in the unit is connected with a verification system that ensures the dose delivery is proceeding as planned and which shuts down the machine if any abnormalities are detected.

2.6. Treatment verification

Treatment verification on our HT unit is performed by software called *Planned Adaptive.* .The software enables the evaluation of the performed treatment using fusion of the planning kVCT image with pre-treatment MVCT image and dose recalculation using the optimized planning sinogram. This process is described in the greater detail in Chapter 3. The fusion of the images can be done using the same techniques that are

accessible in the image registration software installed on the operator station. The viewing of the merged image can give the information about anatomy changes, if they have occurred. In addition, *Planned Adaptive* enables creation of the verification dose for a given fraction that can be further summed to obtain dose delivered over the course of treatment. Once the image fusion is performed the modification of the planning ROIs can be done manually using various tools.

Planned and delivered dose distribution can be compared using DVHs. Software displays summation, planning, or dose difference DVH curve for each ROI. If the result of the comparison is not satisfactory, a new plan can be generated using the treatment planning software to make corrections to the treatment plan and correct for the dose delivery inaccuracies.

Further consideration about this process on HT unit available at Cross Cancer Institute can be found in subsequent chapters.

3. Clinical Outcome for Head and Neck Cancer Treatment

3.1. Head and Neck Cancer Specification

Head and neck (H&N) cancer is a malignant disease, most commonly squamous cell carcinoma and less commonly adenocarcinoma. The malignancy can take its origin in the paranasal sinuses and nasal cavity, the oral cavity, also the nasopharynx, oropharynx, hypopharynx, as well as larynx, and finally lymph nodes in the upper part of the neck. Tumors of the salivary glands and the paranasal sinuses appear less frequently.

The cancer of brain, eye, and thyroid as well as the scalp, skin, muscles, and head and neck bones are not grouped with cancers of the head and neck [Khan et al., 1998; Rubin, 1993].

3.2. Problems in radiation delivery to head and neck tumour

The majority of H&N cancer patients receive radiation therapy. Sometimes it is combined with chemotherapy and/or surgery. The immobilization for radiation treatment

of the H&N patient is usually done using thermoplastic or Perspex masks. The patient positioning problem is not as straightforward as it may seem. There are few sources of positioning uncertainties in H&N cases as indicated by Zhang et al.: (i) the systematic difference between the immobilization device at simulation and at the treatment, (ii) the random setup uncertainties in daily positioning such as residual shifts during the correction process, non rigid movements and rotations of anatomy, and finally (iii) trends caused by anatomic variations which, among others, include tumor shrinkage and/or weight loss as well as physiologic changes during radiotherapy. In addition, Zhang et al. made an observation that the variability in setup shifts for different regions of the anatomy in the H&N site is present and this is involved with head rotations and/or non rigid movement between any two rigid anatomical structures [Zhang et al., 2006].

Other studies indicate that the instabilities in the H&N anatomy are involved with shrinkage of primary tumour or nodal masses, post surgery related changes/edema and, again, weight loss. Those changes can be clinically significant and impact the accuracy of treatment delivery that may consequently lead to underdosage of the tumour due to changes in the PTV and poorer positioning accuracy, or overdosage of the normal tissues, which is especially dangerous for spinal cord or which can lead to a significant quality of life impact in the case of the parotids [Barker et al., 2004; Barkley et al., 1977; Butler et al., 1999; Hansen et al., 2004; Miszczyk et al., 1999; Sobel et al., 1976; Suit et al., 1980]. There are not many papers that describe anatomical changes such as volume shrinkage of the target and OARs as well as weight loss in H&N patients, and the most relevant found in the literature are presented below including other problems such as dose changes and normal tissue complication problem.

For example, Barker et al. [Barker et al., 2004]. conducted a study in order to quantify the changes in the anatomy of H&N cancer patients. The authors evaluated the changes in volume and displacement of primary tumour plus lymph nodes as well as OARs (parotids, spinal canal, mandible and external contour) with respect to the chosen bony structures. Based on the data of 14 H&N patients Barker et al. concluded that measurable anatomic changes were observed during the course of RT. The alternation in the patient' outline, shape, and location of the ROI appeared to be significant during the

second half of treatment that could have resulted with adverse dosimetric effect especially when conformal techniques were used for treatment delivery. Therefore, ART may be useful to maximize the therapeutic ratio of RT.

Another paper, Senkus-Konefka et al, assesses changes in lateral dimensions of irradiated volume in H&N cancer patients and determines the impact of those changes on the dose delivery accuracy. The modification of treatment was observed to be necessary in 30% of the investigated cases due to early radiation reactions and patient weight changes. In addition, Senkus-Konefka et al. concluded that the "*changes of irradiated volume lateral dimensions during H&N cancer radiotherapy may lead to considerable dose delivery inaccuracies*" [Senkus-Konefka et al., 2006].

Bajaj et al. conducted an investigation on HT unit using rigid body registration methods in order to assess GTV and parotid glands volume changes. It was found that GTV volume decreased to an average of 22% of initial volume by sixth week of treatment. Surprisingly, parotid gland volumes revealed an increase in average volume during the first four weeks of therapy and the range among investigated cases was found to be between 64% and 160% of the original volume, with maximal average volume at day 17 of treatment. Finally, average gland volume dropped to 91% (range 73–119%) of the initial volume by 6^{th} week of RT [Bajaj et al., 2006].

The overdosage of the parotids is one of important concerns in H&N treatment since it is a frequent problem in the patients that lose weight significantly and causes number of normal tissue complications in the patients. Eisbruch et al. showed that "*dose/volume/function relationships in the parotid glands are characterized by dose and volume thresholds as well as steep dose/response relationships when the thresholds are reached*" [Eisenbruch et al., 1999], whereas Roesink et al. revealed linear correlation between post radiotherapy salivary flow ratio and parotid gland dose and a strong volume dependency. Also it was found that a mean parotid gland dose should be at least below 39 Gy [Roesink et al., 2001].

One of the most common side effects of excessive irradiation is the impairment of parotid and submandibular glands to produce saliva [Li et al., 2007; Munter et al., 2007; Jha et al., 2000; Valdex, 1991]. For example, it is reported that parotids receiving higher radiation doses produce less saliva. The study made by Li et al. showed that the largest

reduction is present between 1 to 3 months after radiation treatment completion followed by gradual recovery. When mean doses are lower (e.g., <25 Gy), the parotid glands function recovers to pretreatment levels at 12 months and exceeds it at 18 and 24 months. On the other hand, when the parotids receive dose greater than 30 Gy, the stimulated saliva does not recover to original levels after 2 years. Furthermore, according to the data presented in this study, after two years from the treatment completion, the predicted non-simulated saliva is 86% of pretreatment levels for 25 Gy and <31% for >40 Gy [Li et al., 2007].

Munter et al., [Munter et al., 2007] also indicates that the irradiation with the certain dose threshold of the parotid gland may cause a loss in its function to some level. Some patients are given drugs (e. g. Amifostine) to prevent reduced salivary gland function but it is effective only if the certain dose level is not exceeded. However, in this particular study, it was shown that the Amifostine is effective if the patients receive the dose to the parotid glands less than 40.6 Gy [Munter et al., 2007].

Another common side effect experienced by H&N patients is loss of ability to taste. It was found that when the anterior part of the tongue was not irradiated, taste loss was not observed during RT. In addition, the irradiation of the anterior part of the tongue and the consequent taste loss pattern was found to be independent on difference in radiation dose. Furthermore, the taste dysfunction was observed to be just a temporal effect since the recovery of taste loss was seen in both groups four months after completing RT [Yamashita et al., 2006].

In conclusion, the dosimetric effects of anatomy changes in H&N cancer patients indicate that adaptation of the treatment plan for some of the patients that loose a substantial amount of weight is strongly recommended and it is proven by Hansen et al. that "*repeat CT imaging and replanning during the course of IMRT for selected patients with H&N cancer is essential to identify dosimetric changes and to ensure adequate doses to target volumes and safe doses to normal tissues*" [Hansen et al., 2006]. Chapter 3 of this thesis presents an investigation for H&N patients using the *Planned Adaptive* software.

4. Thesis objectives

The objectives of Chapter 2 is to present the statistical evaluation of shifts between kVCT images and MVCT post-treatment images that can determine the net intrafraction patient motion and measure the accuracy and fidelity of image-guided patient positioning. This information can guide and even diminish the margins of the PTV [Stroom et al., 2000] for different sites when compared with the current clinical margins used, after taking into consideration other factors such as immobilization technique and treatment duration. The presented technique can be successfully implemented in-house with the tools available on the HT unit. The statistical analysis of the misalignment shifts obtained from registration of kVCT and post-MVCT image was performed to assess the positioning accuracy of patients with different treatment sites,and to evaluate the appropriateness of the PTV margins. However, these results are a limited set of our own in-house findings and are meant to illustrate the technique, and not to dictate the PTV margin values.

The purpose of Chapter 3 is to assess the dosimetric effects of anatomy changes in H&N cancer patients. It is indicated in the literature that adaptation of the treatment plan for some of the patients that loose weight substantially is strongly recommended [Hansen et al., 2006; Senkus-Konefka et al., 2006]. Due to the limitation of the technique, the interest of the study is focused on the comparison between planned and delivered dose to the OARs, which are, parotid glands, cord and cord plus 5 mm margin. The study also constitutes a feasibility assessment of the *Planned Adaptive* HT software for 'in clinic' use.

Bibliography

Antolak JA, Rosen II, Childress CH, Zagars GK, Pollack A. "Prostate target volume variations during a course of radiotherapy" *Int J Radiat Oncol Biol Phys* 42(3):661-672 (1998).

Antolak JA, Rosen II. "Planning target volumes for radiotherapy: How much margin is needed?" *Int J Radiat Oncol Biol Phys* 44(5):1165-1170 (1999).

Attix FH. "Intoduction to radiological physics and radiation dosimetry" A Wiley-Interscience Publication, John Wiley & Sons (1986).

Bajaj GK, Teslow T, Yu MH, Lee DJ, Ford DJ. "Megavoltage CT assessment of volume changes in target and non-target tissues of the head and neck over a standard course of therapy" *Int J Radiat Oncol Biol Phys* 66(3), Supplement (2006).

Barker JL, Garden AS, Ang KK, O'Daniel J, Wang H, Court LE, Morrison WH, Rosenthal DI, Chao C, Tucker SL, Mohan R, Dong L. "Quantification of volumetric and geometic changes occurring during fractionated radiotherapy for head-and-neck cancer using an integrated CT/linear accelerator system" *Int J Radiat Oncol Biol Phys* 59(4):960–970 (2004).

Barkley HT, Fletcher GH. "The significance of residual disease after external irradiation of squamous-cell carcinoma of the oropharynx" *Radiology* 124:493–495 (1977).

Beavis AW. "Is tomotherapy the future of IMRT?" *British Jour Radiol* 77:285–295 (2004).

Boswell S, Jeraj R, Jaradat H, Mackie TR. "Automatic registration of megavoltage to kilovoltage CT images in helical tomotherapy: An evaluation of the setup verification process for the special case of a rigid head phantom" *Med Phys* 33(11):4395-4404 (2006).

Bracewell RN, The Fourier Transform and its Applications, 2nd ed., McGraw-Hill, New York, (1986).

Butler EB, Teh BS, Grant WH, Uhl BM, Kuppersmith RB, Chiu JK, Donovan DT, Woo SY. "SMART (Simultaneous Modulated Accelerated Radiation Therapy) Boost: A new accelerated fractionation schedule for the treatment of head and neck cancer with intensity modulated radiotherapy" *Int J Radiat Oncol Biol Phys* 45(1):21-32 (1999).

Corbett TH, Valeriote FA, Baker LH. Cytotoxic Anticancer Drugs: Models and Concepts for Drug Discovery and Development. Published 1992 Springer.

Creutzberg AL, Althof VG, Huizenga H, Visser G. "Quality assurance using portal imaging: The accuracy of patient positioning in irradiation of breast cancer" *Int J Radiat Oncol Biol Phys* 25:529-539 (1993).

Delannes M, Daluy J, Bonnet J, Sabatier J, Tremoulet M. "Fractionated radiotherapy of small inoperable lesions of the brain using a non-invasive stereotactic frame", *Int J Radiat Oncol Biol Phys* 21:749 (1991).

Eisbruch A, Haken RKT, Kim HM, Marsch LH, Ship JA. "Dose, volume, and function relationships in parotid salivary glands following conformal and intensity modulated irradiation of head and neck cancer" *Int J Radiat Oncol Biol Phys* 45(3):577–587 (1999).

Fiveash JB, Murshed H, Duan J, Hyatt M, Caranto J, Bonner JA, Popple RA. "Effect of multileaf collimator leaf width on physical dose distributions in the treatment of CNS and head and neck neoplasms with intensity modulated radiation therapy" *Med Phys* 29(6):1116-1119 (2002).

Gao S, Zhang L, Wang H, de Crevoisier R, Kuban D, Mohan R, Dong L. "A deformable image registration method to handle distended rectums in prostate cancer radiotherapy" *Med Phys* 33: 3304 (2006).

Hamilton CS , Eberty MA. "Volumetric Uncertainty in Radiotherapy" *Clinical Oncology* 17: 456–464 (2005).

Hanley J, Lumley MA. "Measurement of patient positioning errors in three dimensional conformal radiotherapy of the prostate". *Int J Radiat Oncol Biol Phys* 37(2):435-444 (1997).

Hansen EK, Bucci MK, Quivey JM, Weinberg V, Xia P. "Repeat CT imaging and replanning during the course of IMRT for head-and-neck cancer "*Int J Radiat Oncol Biol Phys* 64(2):355–362 (2006).

Keller H *et al.*, "Monte Carlo study of a highly efficient gas ionization detector for megavoltage imaging and image-guided radiotherapy," Med Phys **29:**165–175 (2002).

Hill DLG, Batchelor PG, Holden M, Hawkes DJ. "Medical image registration" *Phys Med Biol* 46:R1–R45 (2001).

Hoogeman MS, van Herk M, de Bois J, Lebesque JV. "Strategies to reduce the systematic error due to tumor and rectum motion in radiotherapy of prostate cancer" *Radiotherapy and Oncology* 74:177–185 (2005).

Huntzinger C, Munro P, Johnson S, Miettinen M, Zankowski C, Ahlstrom G, Glettig R, Fillbert R, Kaissl W, Kamber M, Amstutz M, Bouchet L, Klebanov D, Mostafavi H, Stark R. "Dynamic targeting image-guided radiotherapy" *Med Dosimet* 31(2):113-125 (2006).

International Commission on Radiation Units and Measurements. ICRU Report 50: Prescribing, Recording and Reporting Photon Beam Therapy. Bethesda, MD, ICRU (1993).

International Commission on Radiation Units and Measurements. ICRU Report 62 (supplement to ICRU Report 50): Prescribing, Recording and Reporting Photon Beam Therapy. Washington, DC, ICRU (1999).

Jaffray DA, Siewerdsen JH, Wong JW, Martinez AA. "Flat-panel cone-beam computed tomography for image guided radiation" *Int J Radiat Oncol Biol Phys* 53(5):1337–1349 (2002).

Khan FM. "The physics of radiation therapy" 2nd edition, Williams&Wilkins, Baltimore, Maryland (1994).

Khan FM. "The physics of radiation therapy" 3rd edition. Lippincott Williams&Wilkins, Philadelphia (2003).

Khan FM, Potish RA. Treatment Planning in Radiation Oncology. Williams and Wilkins (1998).

Langen KM, Meeks SL, Poole DO, Warner TH, Willoughby TR, Kupelian PA, Ruchala KJ, Haimerl J, Olivera GH. "The usage of megavoltage CT (MVCT) images for dose recomputations" *Phys Med Biol* 2005;50:4259-4276.

Li Y, Taylor JMG, Haken RKT, Eisbruch A."Impact of dose on parotid salivary recovery in head and neck cancer patients treated with radiation therapy" *Int J Radiat Oncol Biol Phys* 67(3):660–669 (2007).

Lia JG, Xing L. "Inverse planning incorporating organ motion" Med Phys 27(7):1573-1578 (2000).

Mackie R, PaltaJ, "Intensity modulated radiation therapy. The state of art:. Medical Physiics Publishing (2003).

Mackie TR, Kapatoes J, Ruchala K, Lu W, Wu C, Olivera G, Forrest L, Tome W, Welsh J, Jeraj R, Harari P, Reckwerdt P, Paliawal B, Ritter M, Keller H, Fowler J, M. Metha.

"Image guidance for precise conformal radiotherapy" *Int J Radiat Oncol Biol Phys* 56(1):89–1349 (2003).

Meeks S, Harmon J, Langen K, Willoughby T, Wagner T, Kupelian P. "Performance characterization of megavoltage computed tomography imaging on a helical tomotherapy unit" *Med Phys* 32(8):2673-2681 (2005).

Miszczyk L, Wydmanski J. "Evaluation of Delivered Dose Changes During Radiation Therapy" *Acta Oncologica* 38(2):197–201 (1999).

Munter MW, Hoffner S, Hof H, Herfarth KK, Haberkorn U, Rudat V, Huber P, Debus J, Karger CP."Changes in Salivary Gland Function After radiotherapy of head and neck tumours measured by quantitaive pertechnetate scintigraphy: Comparison of intensity modulated radiotherapy and conventional radiation therapy with and without amifostine" *Int J Radiat Oncol Biol Phys* 67(3):651–659 (2007)

Pekar V, Gladilin E, Rohr K. "An adaptive irregular grid approach for 3D deformable image registration" *Phys Med Biol* 51:361–377 (2006).

Prisciandaro JI, Frechette CM, Herman MG, Brown PD, Garces YI, Foote RL. "A methodology to determine margins by EPID measurements of patient setup variation and motion as applied to immobilization devices" *Med Phys* 31(11):2978-2987 (2004).

Roesink JM, Moerland MA, Battermann JJ, Hordjik GJ, Terhaard CHJ. "Quantitative dose-volume response analysis of changes in parotid gland function after radiotherapy in the head-and-neck region" *Int J Radiat Oncol Biol Phys* 51(4):938–946 (2001).

Rosu M, Chetty IJ, Tatro DS, Ten Haken RK. "The impact of breathing motion versus heterogeneity effects in lung cancer treatment planning" *Med Phys* 34:1462 (2007)

Rubin P, MacDonald S, Qazi R. Clinical Oncology: A multidisciplinary approach for physicians and students. 7th edition, W.B. Saunders Company (1993).

Ruchala KJ, Oliviera GH, Kapatoes JM. "Limited-data image registration for radiotherapy positioning and verification". *Int J Radiat Oncol Biol Phys* 54(2):592–605 (2002).

Ruchala KJ, Olivera GH, Schloesser EA, Mackie TR, "Megavoltage CT on a tomotherapy system," *Phys Med Bio.* **44**:2597–2621 (1999).

Schell MC, Smith V, Larson Da, Flickinger J, Wu A. "Evaluation of radiosurgery techniques with cumulative dose volume histograms in linac-based stereotactic irradiation", *Int J Radiat Oncol Biol Phys* 20: 1325-1330 (1991).

Scrimger R, Stavrev P, Parliament MB, Field GC, Thompson H, Stavreva N, Fallone BG. "Phenomenologic Model Describing Flow Reduction for Parotid Gland Irradiation with Intensity-Modulated Radiotherapy: Evidence of Significant Recovery Effect", *Int J Radiat Oncol Biol Phys* 60(1):178-185 (2004).

Seargo CF, Houdek PV, Bauer-Kirpes B, Lewin AA, Abitbol AA, Gonzales-Arias S Schwade JG. "Sterotactic radiosurgery: Dose volume analysis of linear accelerator techniques", *Med Phys* 19: 181-185 (1992).

Senkus-Konefka E, Naczk E, Borowska I, Badzio A, Jassem J. "Changes in lateral dimensions of irradiated volume and their impact on the accuracy of dose delivery during radiotherapy for head and neck cancer" *Radiotherapy and Oncology* 79(3):304–309 (2006).

Sobel S, Rubin P, Keller B, *et al.* Tumor persistence as a predictor of outcome after radiation therapy of head and neck cancers. *Int J Radiat Oncol Biol Phys* 1:873–880 (1976).

Sharp L, Lewin F, Johansson H, Payne D, Gerhardsson A, Rutqvist LE. "Randomized trial on two types of thermoplastic masks for patient immobilization during radiation therapy for head-and-neck cancer" *Int J Radiat Oncol Biol Phys* 61:250–256 (2005).

Stroom JC, Olofsen-van Acht MJJ, Quint S, Seven M, De Hoog M, Creutzberg CL, De Boer HCJ, Visser AG. On-line set-up corrections during radiotherapy of patients with gynecologic tumors. Int J Radiat Oncol Biol Phys 46:499–506 (2000).

Suit HD, Walker AM. "Assessment of the response of tumours to radiation: Clinical and experimental studies". *Br Cancer Suppl* 41:1–10 (1980).

Van Dyk J. The modern technology of Radiation Oncology. Madison, Medical Physics Publishing (1999).

Viswanathan AN, Dimopoulos J, Kirisits C, Berger D, Pötter R. "Computed Tomography Versus Magnetic Resonance Imaging-Based Contouring in Cervical Cancer Brachytherapy: Results of a Prospective Trial and Preliminary Guidelines for Standardized Contours" *Int J Rad Oncol Biol Phys* 68(2):491-498 (2007).

Voroney J, Brock KK, Eccles C, Haider M, Dawson LA. "Prospective comparison of computed tomography and magnetic resonance imaging for liver cancer delineation using deformable image registration" *Int J Rad Onc Biol Phys* 66(3):780-791 (2006).

Warkentin B, Stavrev P, Stavreva N, Field C, Fallone BG. "A TCP-NTCP estimation module using DVHs and known radiobiological models and parameter sets". *J Appl Clin Med Phys* 5:50–63 (2004).

Willoughby TR, Kupelian PA, Pouliot J, Shinohara K, Aubin M, Roach M, Skrumeda LL, Balter JM, Litzenberg DW, Hadley SW, Wei JT, Sandler HM. "Target localization and real-time tracking using the calypso 4D localization system in patients with localized prostate cancer" *Int J Radiat Oncol Biol Phys* 65:528-534 (2006).

Yamashita H, Nakagawa K, Nakamura N, Abetakahiro K, Ohmoto A, Okada S, Matsumoto I, Hosoinakashi, Sasano YH, Yamakawa S, Ohtomo K. "Relation between acute and late irradiation impairment of four basic tastes and irradiated tongue volume in patients with head ad neck cancer" *Int J Radiat Oncol Biol Phys* 66(5):1422–1429 (2006).

Yan D, Vicini F, Wong J, Martinez A. "Adaptive radiation therapy" *Phys Med Biol* 42:123–132 (1997).

Yan D, Ziaja E, Jaffray D, Wong J, Brabbins D, Vicini F, Martinez A. "The use of adaptive radiation therapy to reduce setup error: a prospective clinical study" *Int J Radiat Oncol Biol Phys* 41(3): 715–720 (1998)

Yan D., Lockman D, Martinez A, Wong J, Brabbins D, Vicini F, Liang J, Kestin L. "Computed Tomography Guided Management of Interfractional Patient Variation" *Semin Radiat Oncol* 15:168-179 (2005)

Zhang L, Garden AS, Lo J, Ang K, Ahmad A, Morrison WH, Rosenthal DI, Chambers MS, Zhu XR, Mohan R, Dong L. "Multiple regions-of-interest analysis of setup uncertainties for head-and-neck cancer radiotherapy" *Int J Radiat Oncol Biol Phys* 64(5):1559–1569 (2006).

Zierhut D, Flentje M, Frank C, Oetzel D,Wannenmacher M."Conservative treatment of breast cancer: modified irradiation technique for women with large breast" *Radiother Oncol* 31:256-261 (1994).

Chapter 2. Quantifying appropriate PTV setup margins: analysis of patient setup fidelity and intrafraction motion using post treatment megavoltage CT (MVCT) scans

Work published in the IJROBP 68(4):1222-1228 (2007)

1. Introduction

Image-guided radiotherapy (RT) is an emerging option for patient setup and is especially useful in the more advanced forms of radiation delivery, such as intensity-modulated RT (IMRT) in which high-dose gradients and conformal avoidance make patients positioning especially critical. Image guided RT uses three-dimensional images that give precise information about patient position [Jaffray et al., 2002; Ruchala et al., 2002; Yan et al., 1997]. One of the image guided RT and IMRT implementations is that offered by HT, which is a combination of a medical linear accelerator and helical computed tomography (CT) scanner [Beavis, 2004]. HT not only delivers highly conformal IMRT, but also has the ability to perform megavoltage CT (MVCT) on patients before treatment. The software available with the HT unit allows for fusion and registration of MVCT and planning kilovoltage CT (kVCT) data, and patients are repositioned according to these relative image shifts [Langen et al., 2005]. HT also gives the possibility of radiation delivery assessment and its improvement by modification/optimization of the treatment plan [Beavis, 2004; Langen et al., 2005; Mackie et al., 2003]. However, to maximize tumor control and minimize complications in the surrounding tissues, the appropriate definition and choice of the gross tumor volume, CTV, and PTV is needed.

For the critical structures adjacent to high-dose regions, one method to achieve either greater sparing or dose escalation with equal dose to the critical structure is to reduce the margins required for the PTV [Mackie et al., 2003]. This is not an easy task because many factors account for the choice of margin, including the intra- and interfraction motion of organs and patient setup variability [Antolak et al., 1998; Huntzinger et al., 2006; Stroom et al., 2000]. Moreover, if the total tumor volume does

not receive the prescribed dose, some of the cancer cells will survive and the disease will recur [Kinzie et al., 1983; Li et al., 2000; Marks et al., 1974]. Thus, the internal position of the tumor, as well as the positioning accuracy and precision must be known before each treatment session.

The problem of underdosage to the treated region or overdosage to the normal tissue is, however, more complicated than just choosing the appropriate margin definition. It can also occur because of inappropriate patient positioning on the treatment couch. The goal of using patient positioning and immobilization devices is to fix the relationship between the radiation beam and the target, as well as to maintain the position during each treatment session. Skin marks are frequently used in patients for setup purposes. Furthermore, the treatment of specific sites involves particular immobilization techniques [Van Dyk, 2000]. For example, in our center, the prostate patients often have ''modest'' immobilization, which means that only ankle and/or knee rests are used. The most common immobilization device for H&N and glioblastoma multiforme (GBM) cancer patients is a base plate with a facial fixation mask, with the setup reference points marked on them [Van Dyk, 2000]. However, even with a good immobilization device, patient weight loss, which can be a function of time since the first fraction was delivered, can influence the efficacy of any immobilization device.

The statistical evaluation of shifts between kVCT images and MVCT post-treatment images can determine the net intrafraction patient motion and measure the accuracy and fidelity of image-guided patient positioning. This information can guide and even diminish the margins of the PTV [Stroom et al., 2000] for different sites compared with the current clinical margins used, taking into consideration other factors such as immobilization technique and treatment duration. This work demonstrates a technique that can be successfully implemented in-house and that has been based on the tools available with the HT Hi-Art II system available at our centre.

We performed statistical analysis of the misalignment shifts obtained from registration of kVCT and post-MVCT image to assess the positioning accuracy of patients with different treatment sites and evaluated the appropriateness of the PTV margins. It should be emphasized that the results presented are not meant to dictate to

other institutions the appropriate margins for the various sites. These results are simply a limited set of our own in-house findings meant to illustrate the technique.

2. Methods and Materials

Twelve patients with various tumor types were treated at our center using the HT Hi-Art System unit. The patients were treated to different dose levels, depending on the tumor type. Of the 12 patients, 4 had prostate cancer (total dose, 68 or 72 Gy in 25 fractions), 4 had GBM (total dose, 54.4 Gy in 20 fractions), and 4 had H&N cancer (total dose, 60 Gy in 30 fractions, except for 1 patient who received 66 Gy in 33 fractions).

All patients underwent treatment setup on the treatment couch using the appropriate positioning devices (e.g., ankle or knee rest). The H&N and GBM patients also had a more stringent immobilization system (i.e., Perspex or Aquaplast shells). The patients underwent target registration and repositioning according to the fusion of the planning kVCT and pretreatment MVCT for every single fraction. The repositioning was done using appropriate couch shifts in the required directions (the coordinates are defined in Figure 2-1).

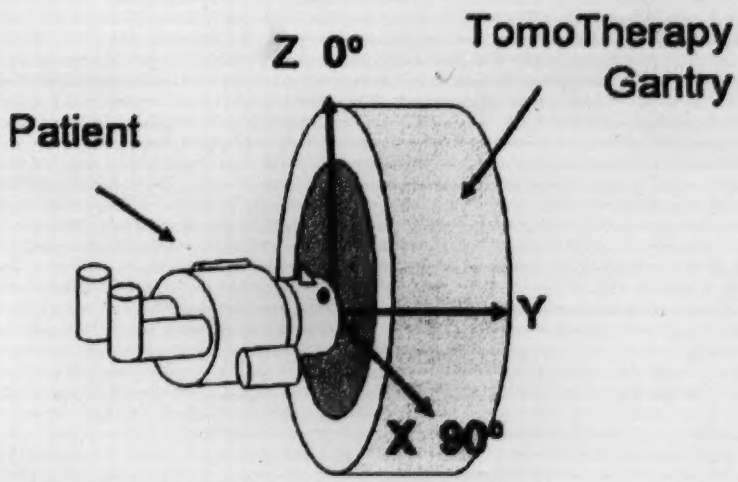

Figure 2-1. Coordinate system on HT unit.

Once the patient/target was appropriately aligned, the treatment was performed. The post-treatment MVCT images were taken once every week for each patient using the on-board MVCT scanner (coarse resolution, 6-mm scan acquisition slice spacing). The post-treatment images were registered with the kVCT images using the TomoTherapy Hi-Art Operator Station, version 2.0.3.52 (Figure 2-2).

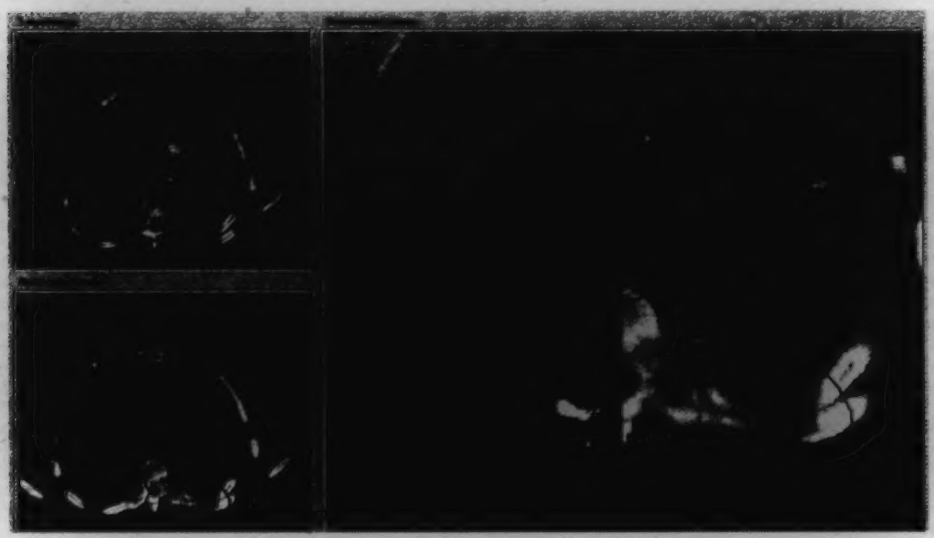

Figure 2-2. Displayed images; a) top left – MVCT image, b) bottom left – kVCT image, c) right – registration of both images, checker example shown in yellow

Depending on the sites being imaged, the operator can select various regions of inclusion to be used by automatic registration to align the MV and kV CT images: (1) bone technique uses only high-density/HU data points from the two image sets; (2) bone and tissue technique uses high- and medium-density/HU data points; and (3) full-image technique uses all data points. In this study, the GBM and H&N patient images were aligned using the first option and the prostate sites were aligned with the bone and tissue registration technique. The HT software also allows one to select the resolution of the images used by the automatic registration process, which determines the number of data points. The registration performed in the study was done using standard resolution, which uses a 4X downsampling of the image in the right–left and suprerior-inferior directions.

The fitting of the images in the study was done using automatic registration, which involves rigid body registration using translations that maximize the mutual information between two image sets. The manual registration of the images was performed by the physicist to verify the accuracy of the automatic registration, and to adjust shifts that were not necessarily attained using automatic bone or tissue matching algorithms, such as in the case of the prostate, which was shifted according to the prostate–rectal interface. Translational shifts defined as the 3D linear offset between kVCT and post-MVCT images were determined from the software. The net radii of the translational shifts were also calculated using a spreadsheet. The averages, standard deviations and medians were calculated for the X, Y, and Z shifts and for the radii. Generally, the median was calculated to give an indication about how much the shifts and radii are affected by any outliers in the data set. The manual data set results were taken to assess the final PTV margins for the prostate for which rigid body geometry cannot be assumed; however, the final margins for the H&N and GBM sites were assessed by taking the greater shift values of the manual and automatic data sets.

The couch readout accuracy was ±0.25 mm; thus, all shifts were rounded to the first decimal place.

3. Results

3.1. Statistics for translations from manual and automatic registration

3.1.1. Automatic registration

Average shifts in the X, Y, and Z directions obtained for different sites in automatic registration are in the positive direction, with the exception of the X coordinate for the prostate. On average, the prostate had the greatest shifts. Moreover, average shift in the Y direction for the prostate was the greatest among all average shifts for registered sites and approached 1 mm. Generally, the smallest shifts were observed in the GBM data (X shifts were close to 0; Table 2-1 and Figures 2-3 – 2-5). Similarly, the greatest standard deviations were obtained for the prostate (maximum, 2.3 mm in the Y direction)

and the smallest for GBM. The standard deviation of the shift was >1 mm in 7 of 9 cases. All median values were within 0.5 mm of the corresponding averages.

3.1.2. Manual registration by physicist

The statistical analysis of the data set obtained by a physicist exhibited not only the same trend, but also nearly the same values as the results for the automatic registration data (Table 2-2 and Figures 2-3 – 2-5). The physicist used the automatic registration as a starting point, and the manual adjustments were an opportunity to double check the automatic registrations and/or adjust the shifts manually. In general, the greatest average shifts and their standard deviations were obtained for the prostate, followed by the H&N and GBM. The standard deviation in the Y direction tended to be the greatest, specifically for the prostate, it reached a maximal value of 2.3 mm. The median values were within 0.5 mm of the corresponding averages.

3.2. Analysis of translations expressed as net radial shift

3.2.1. Automatic registration

The greatest common trend in both data sets was observed when the radial statistics were considered instead of the X, Y, and Z shifts (Table 2-3 and Figure 2-6). The average, median, and standard deviation of the radii were calculated from the shifts for all treated sites.

The average radii and their standard deviations were the largest for the prostate, followed by the H&N and GBM. In general, the automatic data set gave slightly smaller statistical variations for a given treated site compared with the manual data set results. All median values were within 0.6 mm of the corresponding averages.

3.2.2. Manual registration by physicist

The manual data set had a similar outcome as that for the automatic data set (Table 2-3 and Figure 2-6). The greatest average radius and standard deviation was obtained for the prostate and H&N, which were within 0.1 mm of each other in both cases. The GBM data set had the smallest radius and standard deviation at 1.7 and 0.7 mm, respectively. The median for all sites was calculated to be smaller, within about 0.5 mm.

Automatic registration	Prostate N=19			GBM N=13			H&N N=23		
coordinate	x [mm]	y [mm]	z [mm]	x [mm]	y [mm]	z [mm]	x [mm]	y [mm]	z [mm]
Average	-0.4	1.0	0.2	0.0	0.2	0.2	0.2	0.1	0.7
St. dev.	1.6	2.3	1.3	1.2	0.9	0.6	1.1	2.0	1.4
Median	-0.1	0.6	0.3	-0.1	0.2	0.2	0.4	0.0	0.8

Table 2-1. Automatic registration data, N – number of post treatment images

Physicist registration	Prostate N=19			GBM N=13			H&N N=23		
coordinate	x [mm]	y [mm]	z [mm]	x [mm]	y [mm]	z [mm]	x [mm]	y [mm]	z [mm]
Average	-0.6	1.0	0.4	-0.2	0.6	0.1	-0.7	0.4	0.6
St. dev.	1.5	2.3	1.9	1.4	0.8	0.7	1.9	2.0	1.8
Median	-0.2	0.6	1.0	0.0	0.8	-0.1	-0.1	0.6	0.5

Table 2-2. Manual registration data, N – number of post treatment images

site	Prostate Radius [mm] N=19		GBM Radius [mm] N=13		H&N Radius [mm] N=23	
Data set	Automatic	Physicist	Automatic	Physicist	Automatic	Physicist
Average	2.7	2.9	1.4	1.7	2.4	2.8
St. dev.	1.6	2.0	0.6	0.7	1.3	1.9
Median	2.4	2.4	1.5	1.5	1.8	2.2

Table 2-3. Radii obtain from automatic and manual datasets, N – number of post treatment images

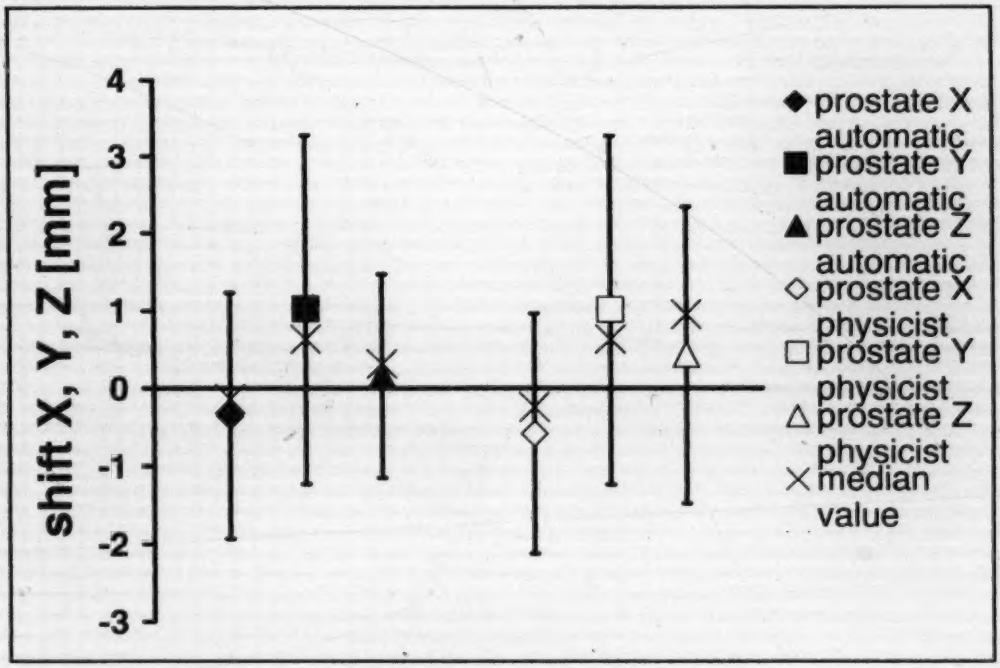

Figure 2-3. Average X, Y and Z shifts for prostate sites

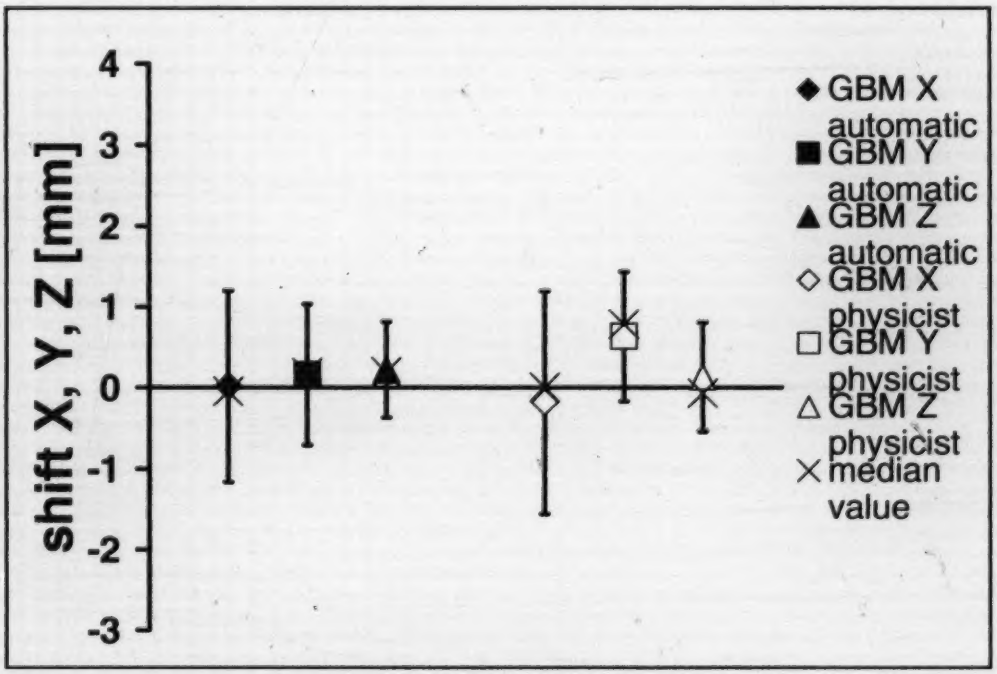

Figure 2-4. Average X, Y and Z shifts for GBM sites

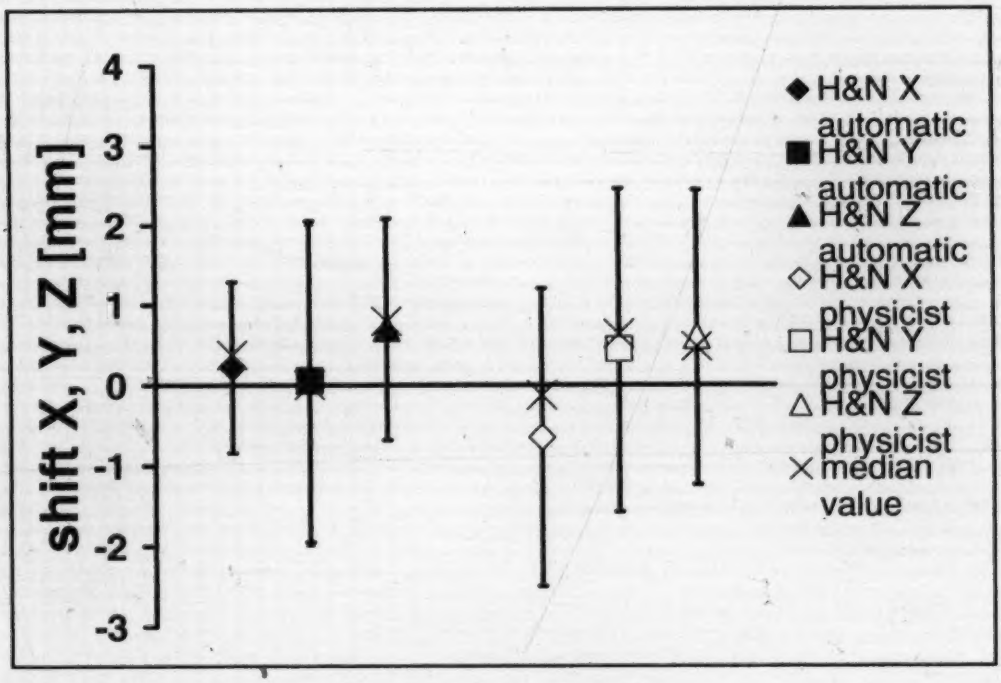

Figure 2-5. Average X, Y and Z shifts for H&N sites

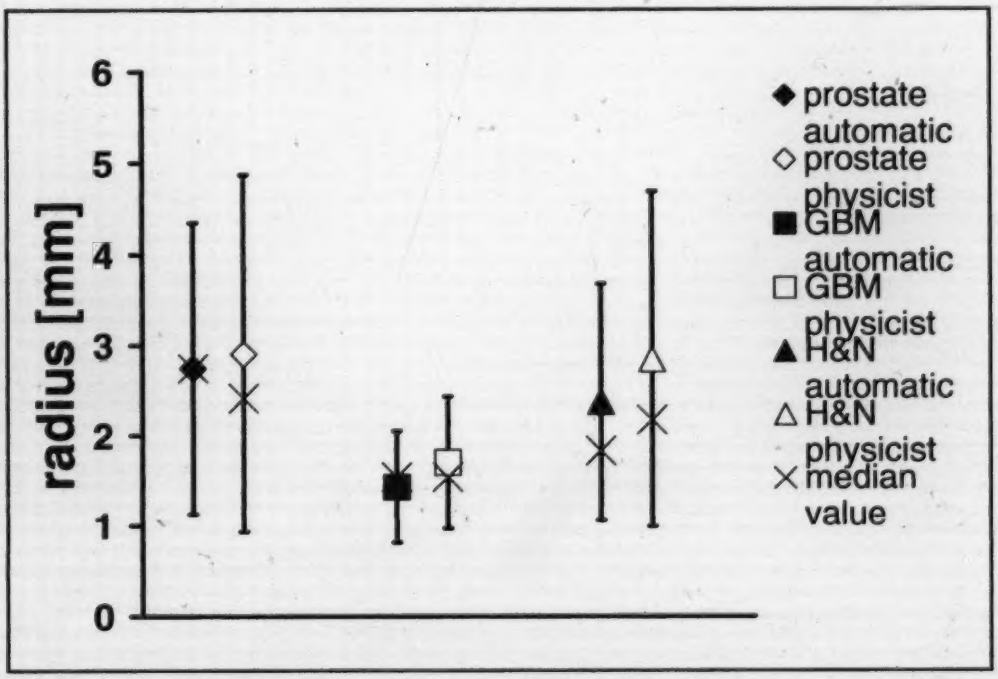

Figure 2-6. Average and median values of radius for prostate, GBM and H&N sites

4. Discussion

4.1. Translations from manual and automatic registration

4.1.1. Prostate

According to the automatic registration data set for the prostate, the average X shift was in the negative direction and the average Z shift in the positive direction, and these were confirmed by the manual data set results. The average Y shift for the prostate was the greatest among all shifts for all sites in both the manual and the automatic data sets. These consistently large values in the data sets of the Y shift and the standard deviation of the Y shift for the prostate were likely in large part due to a lower MVCT scanning resolution in the Y direction, which is limited by the scanning jaw thickness and pitch used in the scanning. This lower resolution might introduce a greater error into the proper alignment of the kVCT–MVCT images in this direction [Mahan et al., 2005].

The median of the shifts was within about 0.5 mm of the corresponding average, indicating that no undue influence resulted from the outliers.

The prostate appeared to have the greatest average shifts, standard deviations, and median values. This could have resulted from a number of factors: (1) the lack of highly constraining immobilization during treatment (knee rest and ankle rest only); (2) movement of the prostate during the course of any given treatment session [Huang et al., 2002; Willoughby et al., 2006]; and (3) and possibly less accurate registration, because the alignment was done not with respect to bone, which is highly visible on the MVCT and kVCT images, but with respect to the rectal–prostate interface, which although visible, is generally not as clearly visible.

4.1.2. Glioblastoma multiforme

According to the data analysis, the GBM shifts were the smallest compared with the other sites. They were less than or equal to 0.5 mm. The median of the shifts, as with the prostate, seemed to indicate that no undue influence of outliers had occurred. The

standard deviations were the smallest of among all the sites and their values were ≤1.2 mm and ≤1.4 mm in the automatic and manual data sets, respectively. In general, the lower shift values resulted because the GBM patients were immoblized with Perspex masks during the course of treatment. Moreover, these patients do not experience the weight loss seen with the other patient population we studied that also use the immobilization mask, namely the H&N patients. Registration was always done for this site with respect to the bony anatomy, because of the character of the site (i.e., a rigid geometric relationship between the treated site and the adjacent bony structures can be assumed).

4.1.3. Head and neck

The average shifts for the H&N sites were always <1 mm. In general, the standard deviations were between 1 and 2 mm. The immobilization masks did not give the same positive outcome as for the GBM patients, most likely because of the noticeable weight loss in the H&N patients.

4.1.4. Automatic and manual data for all sites

Considering the automatic and manual data for all sites, the automatic data set usually had slightly smaller shifts and standard deviations than did the manual data set. The median of the shifts seemed to indicate no undue influence of outliers on the averages. However, the average and median values in both data sets were close to each other and ≤1 mm. Also, the standard deviation in the translational shifts in the Y direction tended to be the largest (four of six times for different sites and registration methods). This was the effect of the coarse resolution of the scanning in this direction. Numerous reports have indicated that the better the resolution of the image is, the more accurate the setup verification using image guidance and as a consequence the more accurate the patient positioning that can be obtained [Boswell et al., 2006; Mahan et al., 2005; Murphy et al., 1999]. Mahan et al. [Mahan et al., 2005] found that the HT image guidance uncertainty in the Y direction was twice as much as the uncertainty in the X and

Y directions using an image resolution of 2.5 mm in the Y direction and 0.7 mm in the X and Z directions. In particular, the 2.5-mm slice thickness results in an uncertainty on the level of submillimeters (s = ±0.6 mm). According to the tendency indicated by Mahan et al. [Mahan et al., 2005], it can be expected that the uncertainty of the imaging system using a 6 mm slice thickness would be greater than the submillimeter level. This was confirmed by Boswell et al. [Boswell et al., 2006] whose data revealed that the imaging error using a coarse scanning resolution was, roughly, ≥1 mm. Therefore, caution should be taken when analyzing the Y shift values displayed by the software after registration because they will always be given with submillimeter accuracy.

Regarding appropriate margins for intrafraction motion, in general, it is most likely appropriate to use a margin equal to two standard deviations of the average shift value in order to obtain 95% confidence in the choice of the appropriate margin [Antolak at al., 1998; Antolak et al., 1999]. Although one could apply a symmetric margin to the sites studied using the radial shifts (symmetric approach), given what appears to be a slightly greater uncertainty in the Y direction, it might be more appropriate in the HT image guided adaptive radiotherapy (IGAR) case to use an asymmetric shift applied in the X, Y, and Z directions.

4.2. Translations expressed as net radial shift

The radial analysis for the sites among the registration data sets confirmed most of the general observations noted in the shift analysis. For all sites, the calculated radii for the prostate were the greatest and those for GBM the smallest. The average radial values ranged from about 1.4 to 2.9 mm when taking into consideration both data sets. The standard deviation was usually greatest for the prostate and smallest for GBM. The median of the radial shifts again seemed to indicate that no undue influence of outliers had occurred.

4.3. Limitations

The presented method has a limitation because any error from the pretreatment MVCT registration will be carried over to the subsequent post-treatment registration. This is a consequence of the assumption that, after repositioning of the patient according to the pretreatment MVCT fusion, an ideal alignment will have been obtained. However, registration of the post-treatment MVCT with the pretreatment MVCT would certainly provide more accurate information about positioning accuracy and net intrafraction motion, because the registration error from the pretreatment images would not be reproduced by default. However, this is not easily realized, because it is not one of the options available in the software.

5. Conclusion

We used post-treatment MVCT to assess the net intrafraction motion and patient setup fidelity, as well as the appropriateness of margins added to the CTV using post treatment image registration. The additional data set gathered by the physicist is important for assessing the appropriateness of the automatic registration performed with the software, in the cases in which rigid fusion is appropriate, and to refine the registration in the cases in which it is not (e.g., the prostate). The comparison of the results obtained for both data sets demonstrated the sufficiency of using the automatic data set to determine the PTV margins because the values of the shifts and the statistical data were nearly equal.

Also, even the modest immobilization cases (e.g., prostate, palliative treatment) had average translational shifts according to the post-treatment scan within 1 mm, and no large outliers were noted (i.e., the medians of the shifts were close to the averages). Additionally, the setup accuracy and setup fidelity seemed to be generally acceptable, because the shifts in all directions and for all sites were within 1 mm.

According to the reference data set, the appropriate margins for our institute and for setup fidelity and intrafraction motion in the GBM and H&N cases are calculated by multiplication of standard deviation of a given shift by the factor of 2. They appeared to

be about 3–4 mm in the X direction and 2–4 mm in the Z direction. For the H&N, the Y margins should be 4 mm, and for GBM, they should be 2 mm. For the prostate, the appropriate margins for setup fidelity and intrafraction motion appeared to be about 3 mm in the X direction, 4 mm in the Z direction, and 5 mm in the Y direction.

In general, the analysis of both data sets resulted in large values of Y shift and large standard deviation owing to the lower resolution of the images in the Y direction.

We have presented our preliminary data and further investigation is needed. However, this method could also be applied using individual patient post image scanning and combined with adaptive planning to reduce or increase margins as appropriate. The results we have presented represent our experience using this technique. Although our values could be used as a guideline for appropriate margins, the same technique could be used by any suitably equipped center (i.e., with three-dimensional imaging available on the treatment unit) to assess site-specific margins by performing post-treatment imaging. The time involved in performing such post treatment imaging, and assessing the results, need not be overly onerous (about 3–5 min), and the frequency of the post-treatment imaging would be at the discretion of the facility (daily, weekly, and so forth) depending the available time in a treatment slot.

Bibliography

Antolak JA, Rosen II. "Planning target volumes for radiotherapy: How much margin is needed?" *Int J Radiat Oncol Biol Phys* 44(5):1165-1170 (1999).

Antolak JA, Rosen II, Childress CH, Zagars GK, Pollack A. "Prostate target volume variations during a course of radiotherapy" *Int J Radiat Oncol Biol Phys* 42(3):661-672 (1998).

Beavis W. "Is tomotherapy the future of IMRT?" *The British J of Radiol* 77:285–295 (2004).

Boswell S, Tome W, Jeraj R, et al. "Automatic registration of megavoltage to kilovoltage CT images in helical tomotherapy: An evaluation of the setup verification process for the special case of a rigid head phantom" *Med Phys* 33: 4395–4404 (2006).

Hamilton CS, Eberty MA. "Volumetric uncertainty in radiotherapy" *Clin Oncol* 17:456–464 (2005).

Huang E, L Dong L, A Chandra A, D A Kuban DA, I I Rosen II, A Evans A, A Pollack A. "Intrafraction prostate motion during IMRT for prostate cancer" *Int J Radiat Oncol Biol Phys* 53(2):261-268 (2002).

Huntzinger C, Munro P, Johnson S, Miettinen M, Zankowski C, Ahlstrom G, Glettig R, Fillbert R, Kaissl W, Kamber M, Amstutz M, Bouchet L, Klebanov D, Mostafavi H, Stark R. "Dynamic targeting image-guided radiotherapy" *Med Dosimet* 31(2):113-125 (2006).

International Commission on Radiation Units and Measurements. ICRU Report 50: Prescribing, Recording and Reporting Photon Beam Therapy. Bethesda, MD, ICRU 1993.

International Commission on Radiation Units and Measurements. ICRU Report 62 (supplement to ICRU Report 50): Prescribing, Recording and Reporting Photon Beam Therapy. Washington, DC, ICRU 1999.

Jaffray DA, Siewerdsen JH, Wong JW, Martinez AA. "Flat-panel cone-beam computed tomography for image guided radiation" *Int J Radiat Oncol Biol Phys* 53(5):1337–1349 (2002).

Kinzie J, Hanks G, Maclean C, Kramer S. "Patterns of care study: Hodgkin's disease relapse rate and adequacy of portals" *Cancer* 52:2223-2226 (1983).

Langen KM, Meeks SL, Poole DO, Warner TH, Willoughby TR, Kupelian PA, Ruchala KJ, Haimerl J, Olivera GH. "The usage of megavoltage CT (MVCT) images for dose recomputations" *Phys Med Biol* 50:4259-4276 (2005).

Li JG, Xing L. "Inverse planning incorporating organ motion" *Med Phys* 27(7):1573-1578 (2000).

Mackie TR, Kapatoes J, Ruchala K, Lu W, Wu C, Olivera G, Forrest L, Tome W, Welsh J, Jeraj R, Harari P, Reckwerdt P, Paliawal B, Ritter M, Keller H, Fowler J, M. Metha. "Image guidance for precise conformal radiotherapy" *Int J Radiat Oncol Biol Phys* 56(1):89–1349 (2003).

Marks J, Davis M, Haus A. "Anatomic and geometric precision in radiotherapy" *Radiol Clin Biol* 43:1-20 (1974).

Mahan SL, Ramsey CR, Scaperoth DD, et al. "Evaluation of image guided helical tomotherapy for the retreatment of the spinal metastasis". *Int J Radiat Oncol Biol Phys* 63: 1576–1583 (2005).

Murphy MJ. "The importance of computed tomography slice thickness in radiographic patient positioning for radiosurgery" *Med Phys* 26:171–174 (1999).

Prisciandaro JI, Frechette CM, Herman MG, Brown PD, Garces YI, Foote RL. "A methodology to determine margins by EPID measurements of patient setup variation and motion as applied to immobilization devices" *Med Phys* 31(11):2978-2987 (2004).

Ruchala KJ, Oliviera GH, Kapatoes JM. "Limited-data image registration for radiotherapy positioning and verification" *Int J Radiat Oncol Biol Phys* 54(2):592–605 (2002).

Stroom JC, Olofsen-van Acht MJJ, Quint S, Seven M, De Hoog M, Creutzberg CL, De Boer HCJ, Visser AG. "On-line set-up corrections during radiotherapy of patients with gynecologic tumors" *Int J Radiat Oncol Biol Phys* 46:499–506 (2000).

Van Dyk J. The Modern Technology of Radiation Oncology: A Compendium for Medical Physicists and Radiation Oncologists. Medical Physics Publishing, Madison, WI; 1999.

Willoughby TR, Kupelian PA, Pouliot J, Shinohara K, Aubin M, Roach M, Skrumeda LL, Balter JM, Litzenberg DW, Hadley SW, Wei JT, Sandler HM. "Target localization and real-time tracking using the calypso 4D localization system in patients with localized prostate cancer" *Int J Radiat Oncol Biol Phys* 65:528-534 (2006).

Yan D, Vicini F, Wong J, Martinez A. "Adaptive radiation therapy" *Phys Med Biol* 42:123–132 (1997).

Chapter 3. Dose Delivery Assessment for Head and Neck Cancers Using *Planned Adaptive* Helical Tomotherapy Software

1. Introduction

The majority of patients with cancer in the H&N region (e.g. cancer of the sinuses, nasopharynx, base of tongue, larynx, etc.) receive radiation therapy (RT). Sometimes this treatment is combined with chemotherapy and/or surgery. The immobilization for radiation treatment of the H&N patient is usually done using molded Perspex or thermoplastic masks. The problem of consistently positioning the patient in a reproducible way is not as straightforward as it may appear. There are several sources of positioning uncertainties in H&N cases as indicated by Zhang et al.: (i) the systematic difference between the utilization of immobilization device at simulation and at the treatment; (ii) the random setup uncertainties in daily positioning such as residual shifts during the correction process, non rigid movements and rotations of anatomy; and finally (iii) trends caused by anatomic variations as well as physiologic changes during radiotherapy. In addition, Zhang et al. made the observation that variability in setup shifts for different regions of the anatomy in the H&N site may be present and could involve such things as head rotations and/or non rigid movement between rigid anatomical structures [Zhang et al., 2006].

In particular, a number of studies indicate that the instabilities in the H&N anatomy are due to such things as shrinkage of primary tumour or nodal masses, post surgery related changes/edema and weight loss. Those changes can be clinically significant and can impact the accuracy of treatment delivery that, as a consequence, may lead to underdosage of the tumour due to alternation in PTV location / extent and poorer positioning accuracy, or may lead to overdosage of the normal tissue, which can in turn lead to unacceptable morbidity for structures such as the parotids and spinal cord [Barker et al., 2004; Barkley et al., 1977; Butler et al., 1999; Hansen et al., 2004; Miszczyk et al., 1999; Sobel et al., 1976; Suit et al., 1980]. In contrast, there are not many papers that describe anatomical changes such as volume changes of the target and organs at risk (OARs) and weight loss in H&N patients. For example, Barker et al. conducted a study in

order to quantify the changes in the anatomy of H&N cancer patients. The method designed in this project allowed assessment of changes in volume and displacement of primary tumour plus lymph nodes as well as OARs (parotids, spinal canal, mandible and external contour) with respect to the chosen bony structures. It was found that the gross tumour volume (GTV) decreased at a median rate of 1.8%/treatment day, the range was 0.2–3.1%/day and the median total relative loss was equal to 69.5% of the initial GTV, the range was 9.9–91.9%. In addition, the median center of the mass displacement was equal to 3.3 mm with the range of 0–17.3 mm. Also the decrease in the volume of parotid glands (median = 0.19 cm^3/d range = 0.04–0.84 cm^3/d) and displacement mostly in the medial direction (median = 3.1 mm; range = 0–9.9 mm) was also observed. In addition, the shift in the location of the parotid glands correlated highly with the patient weight loss that occurred during treatment [Barker et al., 2004].

Another paper that describes the anatomy changes assessment in H&N patients was published by Senkus-Konefka et al. The modification of treatment was observed to be necessary due to early radiation reactions and patient weight changes. The authors of the paper noticed that the requirement of RT accessory modification was correlated with the amount of weight loss during treatment [Senkus-Konefka et al., 2006]. Consequently, this is another study that indicates the real importance of treatment adaptation for H&N sites.

The overdosage of the parotids is an important concern in H&N treatment since it is a frequent problem in the patients that lose weight significantly. It can result normal tissue complications in the patients [Eisenbruch et al., 1999], and Roesink et al. noted a linear correlation between post salivary flow rate and parotid gland dose. In addition, a strong dependency of parotid salivary flow after radiation and the fraction of the parotid gland irradiated was observed. Some studies have found that a mean parotid gland dose should be below 39 gray (Gy) [Roesink et al., 2001], however, other studies indicate that it should be less than 25 Gy [Scrimger et al., 2004, Warkentin et al., 2004]..

One of the most common side effects is the parotids' impairment to produce saliva. It is reported that parotids receiving higher radiation produce less saliva. The study performed by Li et al. showed that the largest reduction is present between 1 to 3 months

after radiation treatment completion followed by gradual recovery. When mean doses are lower (e.g., <25 Gy), the parotid glands function recovers to pretreatment levels at 12 months and exceeds it at 18 and 24 months. On the other hand, when the parotids receive dose greater than 30 Gy, the stimulated saliva does not recover to original levels after 2 years. Furthermore, according to the data presented in this study, after two years from the time of treatment completion, the predicted two-year post-treatment non-simulated saliva is 86% of pretreatment levels for 25 Gy and <31% for >40 Gy [Li et al., 2007].

Another study carried out by Munter et al. also indicates that the partial loss of function of the parotid gland depicts dose threshold under radiation therapy. Some patients are given drugs (e. g. Amifostine) to prevent reduced salivary gland function but it is effective only if the mean parotid dose is less than 40.6 Gy [Munter et al., 2007].

Another common side effect experienced by H&N patients is taste loss. It was found that when the anterior part of the tongue was not irradiated, taste loss was not observed during RT. In addition, the irradiation of the anterior part of the tongue and the consequent taste loss pattern was found to be independent of radiation dose. Furthermore, the taste dysfunction was observed to be just a temporary effect [Yamashita et al., 2006].

In conclusion, the dosimetric effects of anatomy changes in H&N cancer patients may lead to unwanted normal tissue complications. The adaptation of the treatment plan for some of the patients that lose weight substantially is strongly recommended and Hansen et al. have reported that replanning during the course of IMRT for selected H&N cancer patients is essential to identify dosimetric changes and to ensure adequate doses to target volumes and safe doses to normal tissues [Hansen et al., 2006].

Chapter 3 of this thesis presents an investigation done for H&N patients on HT unit using the TomoTherapy *Planned Adaptive* software. The presented study is designed to assess the dosimetric effects of anatomy changes in H&N cancer patients by comparing the dose delivered to the PTV 60, PTV 54, parotid glands, spinal cord and cord plus 5 mm margin, that is obtained by recalculation of planning sinogram on merged images, to the planned doses to the same VOIs that were calculated by the treatment planning software before first fraction was delivered. This work also constitutes a feasibility assessment of the *Planned Adaptive* Tomotherapy software for 'in clinic' use.

2. Methods and Materials

A total of twelve H&N patients completed treatment at the time of the start of this analysis on a HT Hi-Art treatment unit according to an in house radiation therapy protocol (see selected goals of the protocol that were used in this study in Table 3-1). Each patient received 60 Gy in 30 fractions to the PTV60 over the period of approximately 6 weeks. Pre-treatment megavoltage computed tomography (MVCT) images were acquired before delivery of each fraction for patient positioning purposes (image guidance). Patients were immobilized using a molded Perspex or thermoplastic facial mask and once the positioning of the patient was satisfactory the treatment was performed.

VOI	Treatment Goal 1	Treatment Goal 2	Treatment Goal 3
PTV60	90% of PTV60 to receive 60Gy (by definition) 99% of volume at or above 54 Gy 20% of volume at or below 66.0 Gy	≤ 1% of PTV60 to receive ≤ 54Gy (cold spot)	≤ 20% of PTV60 to ≥ 66Gy (hot spot)
PTV54	90% of PTV54 to receive ≥ 54Gy		
Parotid L And Parotid R	50% of one or both parotids to receive ≤ 30Gy		
Cord	Max dose ≤ 45Gy		

Table 3-1. H&N treatment protocol dose constraint analysis points

The assessment of the treatment delivery was done using the *Planned Adaptive* HT Hi-Art software (v. 2.2.1.2.12). The pre-treatment MVCT image was merged with the original planning kVCT image using the relative shifts calculated at the time of treatment using rigid body image registration. These shifts between the images were stored in the HT database and loaded at the time of merging. The MVCT images were inserted into

kVCT image in their proper registered location, using the image shifts from the database (rotations were not taken into account), and the remaining slices being supplied those from the original planning kVCT image. This process was repeated for each analyzed fraction. Since the effect of shrinkage in the patient on the dose delivery was investigated in the study and the software is capable of rigid body registration and non-deformable dose summation only, the dose summation analysis had to be for delivered fractions in which patient's anatomy had stabilized (i.e. patients could not be experiencing any significant continued shrinkage for the fractions where we wished to sum the delivered doses). The requirement of stabilized anatomy was imposed in order to obtain more accurate dose verification data, since the verification dose was calculated for each fraction merged image using the same ROIs and then the dose distribution of each fraction were summed. Since only non-deformable dose summation is available in the software, in order to be completely accurate, the assumption has to be made that the patient anatomy is unchanging.

The preliminary assessment of the anatomy stabilization (i.e. cessation of shrinkage) is done by choosing a transverse slice representative of the shrinkage and measuring the magnitude of the shrinkage by taking the length reading of the planned and present outlines of patient's skin in the left – right direction using a measuring tool available in the software. If the length measurement were found to be constant over a number of fractions, the patients were assumed to be stable. According to this selection process, only five patients had stabilized toward the end of their course of treatment (after 10 to 25 fractions of the full course of 30 fractions).

Further shrinkage assessment was done for the selected H&N cases in order to find the exact number of fractions that were delivered to the stabilized anatomy. The manual re-contouring or contour adjustment of PTV60, PTV54, cord, cord plus 5 mm and parotid glands was performed when required on each slice; this re-contouring was done by a physics graduate student, and reviewd by a radiation oncologist. Since the merged image has a low resolution and poor soft tissue contrast, the adjustment of PTV contours was done to the contour of the patient's body surface. As a consequence the volume change was observed if the original PTV contour was outside the current patient outline. The outline of the parotids was not easily visible, so re-contouring was done using the

guidance of the original contour, the distance from the patient outline and the position relative to the mandibles. In the case of cord and of the cord plus 5 mm margin, the volume change was not observed at all, however shifting of the contours was often necessary in order to account for the changes in the spinal cord position. Once re-contouring was completed, the volume assessment of all regions of interest (ROI) mentioned above was performed based on contours for each analyzed fraction. The average shrinkage (i.e. volume change per fraction) in stabilized anatomy with respect to the initial anatomy was calculated using linear regression analysis. In addition, a standard deviation of the slope for each ROI was computed using least squares fitting formula. Due to the fact that stable anatomy is assumed and each measurement is expected to measure the same volume value (the slope should be, ideally, equal 0) each data point has the same standard deviation.

As mentioned before, in order to compare the re-calculated dose for each analyzed fraction and the planned dose, the patient anatomy had to be stable meaning that the shrinkage among analyzed fractions had to be close to 0 which means that the patient's anatomy remains unchanged. A further simple statistical assessment of the patient anatomy was also performed. It was assumed that the anatomy was statistically stable (i.e. the volume change of given ROI was not statistically significant) when the slope of the trend line was within two standard deviations of zero. Consequently, this means that the average change of the volume of ROI must have been smaller than two standard deviations to have 95% confidence level for the measurements, assuming normal distribution of the volume readings

. In order to review the dose delivery, the verification doses as well as summation dose had to be calculated. The verification dose is obtained by recalculation of the dose using the original planned radiation treatment (i.e. planning treatment sinogram that is assumed to be equal to delivered sinogram) projected onto the merged image (i.e. the daily image). This enables recalculation of the dose that more accurately represents the delivery of single fraction from a given day. The summation dose is obtained by summation of verification doses of individual fractions, and which is displayed on one representative merged image. Using that merged image along with its associated adaptive contours we can recalculate the DVH for those summed fractions. In this study the

representative merged image for a given patient was chosen to be the one with the greatest number of MVCT slices among MVCT images available in analyzed fractions. In three cases the representative image was taken in the earliest delivered fractions eligible for analysis whereas in the remaining cases the image was taken from the dataset of the last delivered fraction. However, due to the fact that the stable anatomy during the time where the analyzed fractions were delivered is assumed any of the images can be chosen to perform dose summation.

Once summation doses for analyzed fractions are obtained, they are subsequently extrapolated to the full course of treatment (i.e. summed DVH doses are scaled by {total fx #}/{# fx summed}) in order to give a worst case scenario in terms of the outcome for the full course of treatment. Once the final DVH for dose delivery was obtained its values were compared with the constraint values defined in the protocol. The percentage dose difference was calculated between the delivered and planned dose and data analysis was performed using the following formula: 100 x (summed dose – planned dose) / planned dose.

3. Results

3.1. Volume analysis

There are a significant number of fractions that are assumed to be stable according to the preliminary assessment in *Patient 1*. In this case, the PTV 54 and PTV60 are large in comparison to other patients and visible shrinkage areas are not always fully covered by MVCT image. In addition, the extent of the incomplete coverage is variable. This is expected to influence the volume analysis for PTVs. Linear regression of the volume readings for this patient gives the following results (Table 3-2, Figure 3-1 – 3-4): the volumes of the PTV60 and the PTV54 are roughly constant. The slope of both PTV60 and PTV54 are about -0.57cc/fraction. If the slope is within two standard deviations of zero for given VOI is assumed to be stable. Since the average slope is within two standard deviations of zero for both PTVs, the VOIs in this case are deemed to be stable. It is assumed that the volumes remain constant over the fractions used for dosimetric

evaluation. According to the shrinkage evaluation, stabilization of the anatomy is observed early on during the course of treatment, around the 10th fraction (30 fractions are delivered in total).

The volume changes in the parotids are also scattered around a roughly constant value and there is no strong decreasing or increasing trend. The parotids are statistically stable in terms of their volume changes. The slope of the best fit line is nearly 0 in both cases; the values are equal to -0.02 cc/fraction for the right and 0.04 cc/fraction for the left parotid. The volume of the left parotid on average decreased by 19% of its initial volume during the course of treatment whereas the right parotid lost about 6% of its initial volume. The asymmetric volume loss in the parotids can be related to the fact that the PTV60 is located on the left side of the HN area. Overall, *Patient 1* is deemed to be eligible for dose recalculation for the chosen fractions.

Patient 1				
	PTV60	PTV54	Left parotid	Right parotid
initial volume (cc)	499.1	904.6	16.36	21.76
Slope (cc / fx)	-0.6	-0.6	0.04	-0.02
slope error (cc / fx)	0.4	0.4	0.06	0.04
Intercept (cc)	485	888	13	20.8
intercept error (cc)	9	9	1	0.8
R^2	0.08	0.08	0.02	0.02

Table 3-2. Linear regression results of VOIs for Patient 1

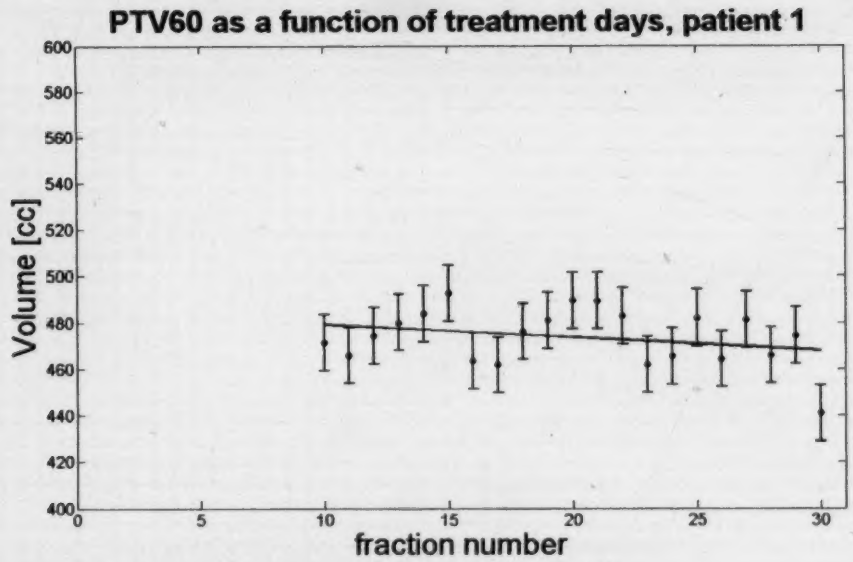

Figure 3-1. Linear regression for the PTV 60, Patient 1

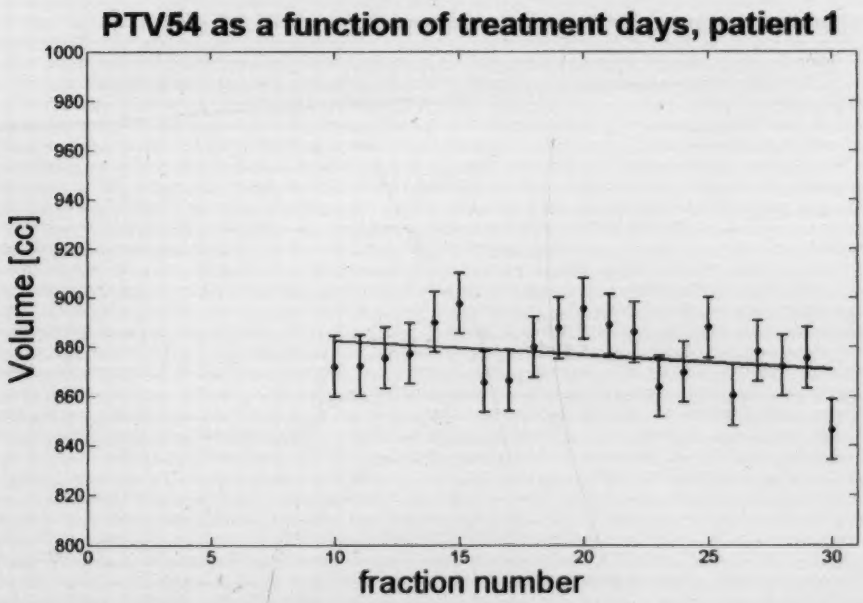

Figure 3-2. Linear regression for the PTV 54, Patient 1

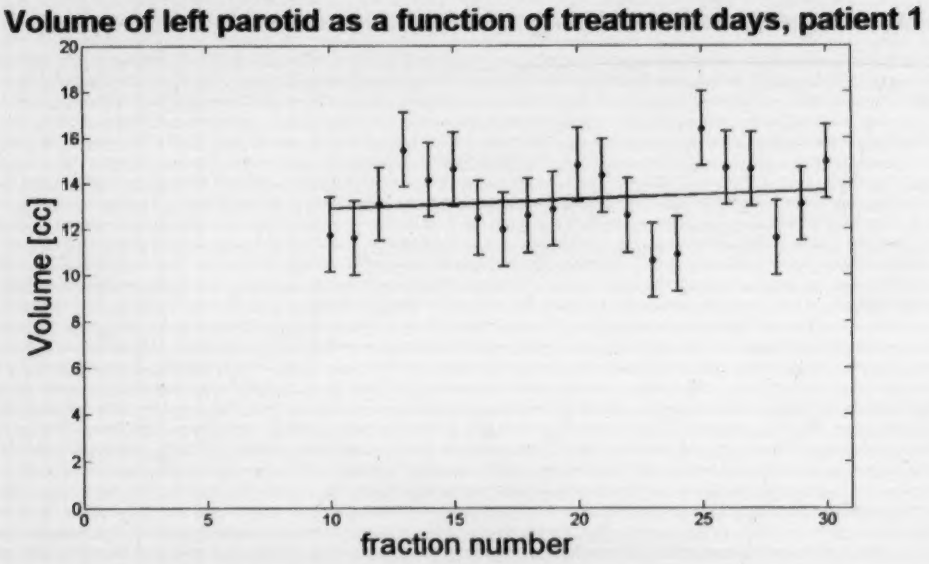

Figure 3-3. Linear regression for the volume of left parotid, Patient 1

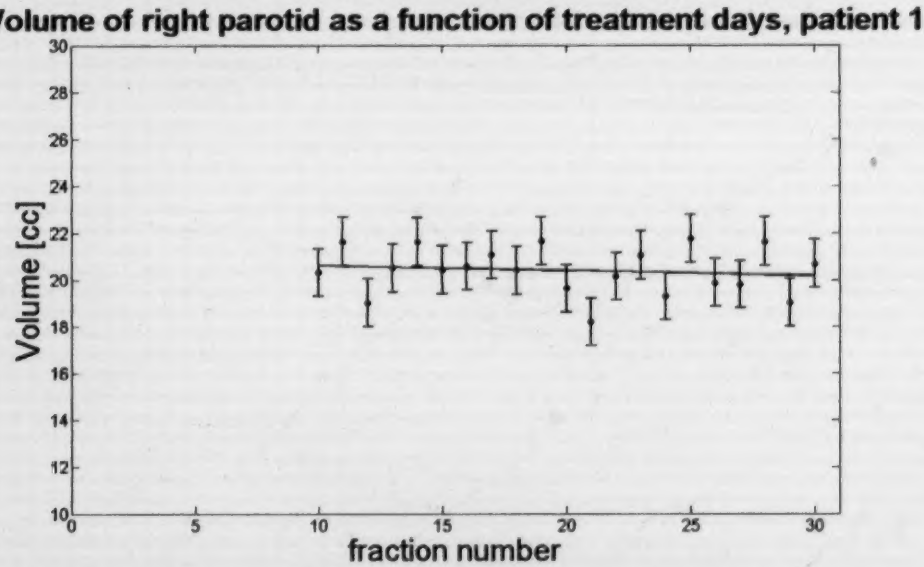

Figure 3-4. Linear regression for the volume of right parotid, Patient 1

In general, *Patient 2* did not experience significant shrinkage and anatomy stabilization occurred late in the treatment course (25th fraction) (Table 3-3, Figure 3-5 – 3-8). The results of the linear regression of PTV values in *Patient 2* indicate that they are not statistically stable. The slope of the PTV60 is close to 0, however, it is positive (0.09

cc/fraction) which seems to be rather unlikely since the PTV is expected to decrease over the course of treatment. On the other hand, the slope of the PTV54 is statistically significant with a value of -2.2 cc/fraction.

The change in parotid volumes is not significant and the values are equal to 0.2 cc/fraction and -0.1 cc/fraction for the left and right parotid respectively. In addition, the positive slope for the volume of the left parotid is not realistic, as again, the volume is expected to remain the same or decrease over the course of treatment. The total percentage loss with respect to the initial volume is equal to 17.25% for the left parotid and 3.7% for the right parotid. Overall, the patient is considered to be eligible for dose recalculation for the chosen fractions.

Patient 2				
	PTV60	PTV54	Left parotid	Right parotid
initial volume (cc)	181.77	1160.4	21.7	26.1
Slope (cc / fx)	0.09	-2.2	0.2	-0.1
slope error (cc / fx)	0.03	0.9	0.2	0.2
Intercept (cc)	179	1210	12	29
intercept error (cc)	1	24	6	4
R^2	0.6	0.6	0.2	0.2

Table 3-3. Linear regression results of VOIs for Patient 2

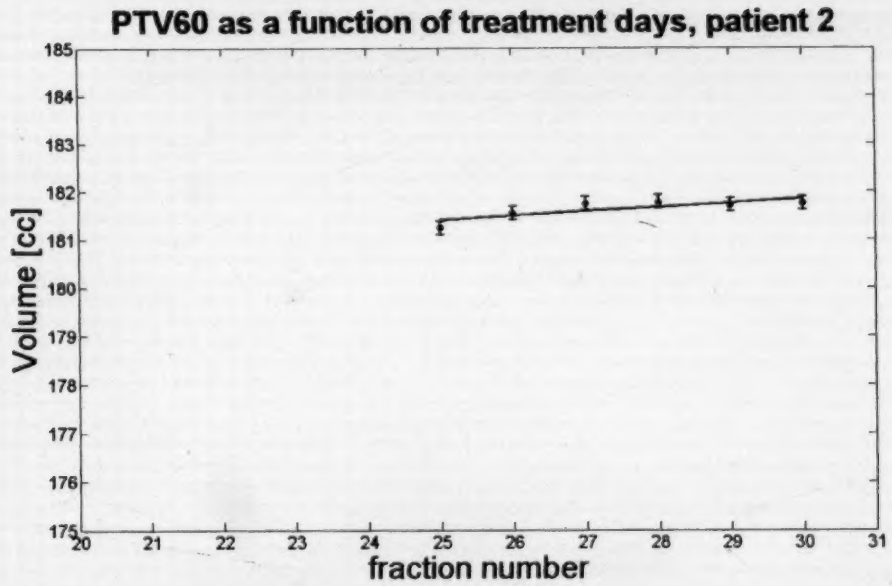

Figure 3-5. Linear regression results for PTV60 for Patient 2

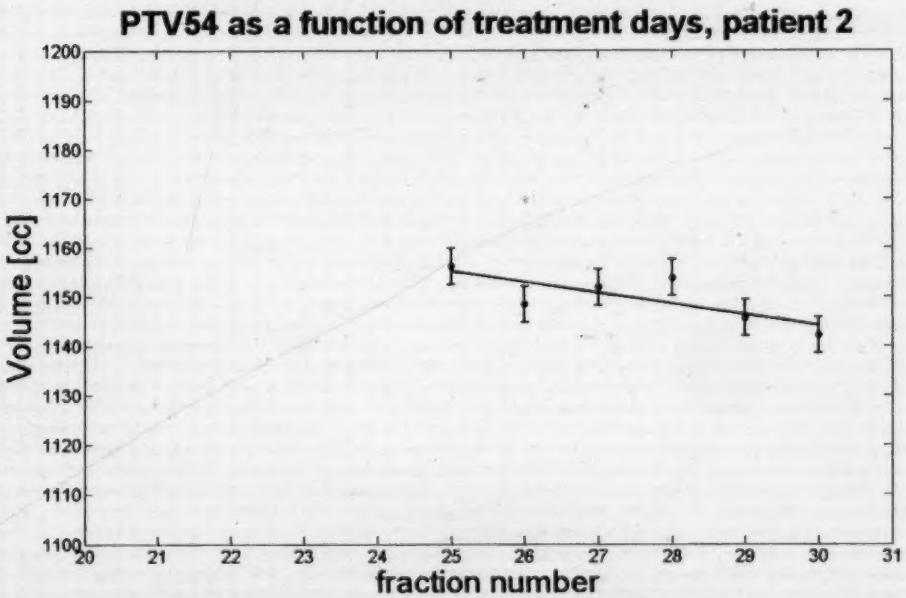

Figure 3-6. Linear regression results of the PTV54 for Patient 2

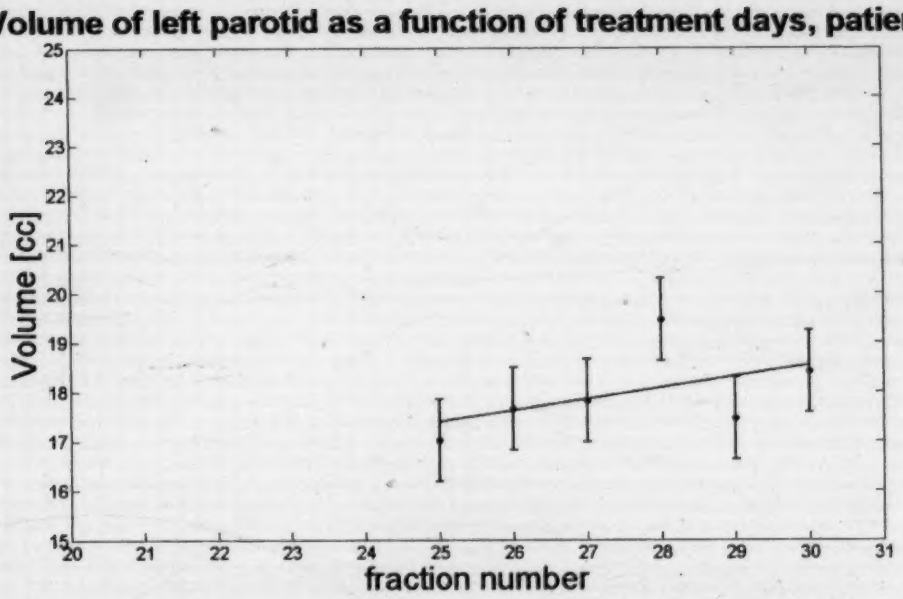

Figure 3-7. Linear regression results of the volume of left parotid for Patient 2

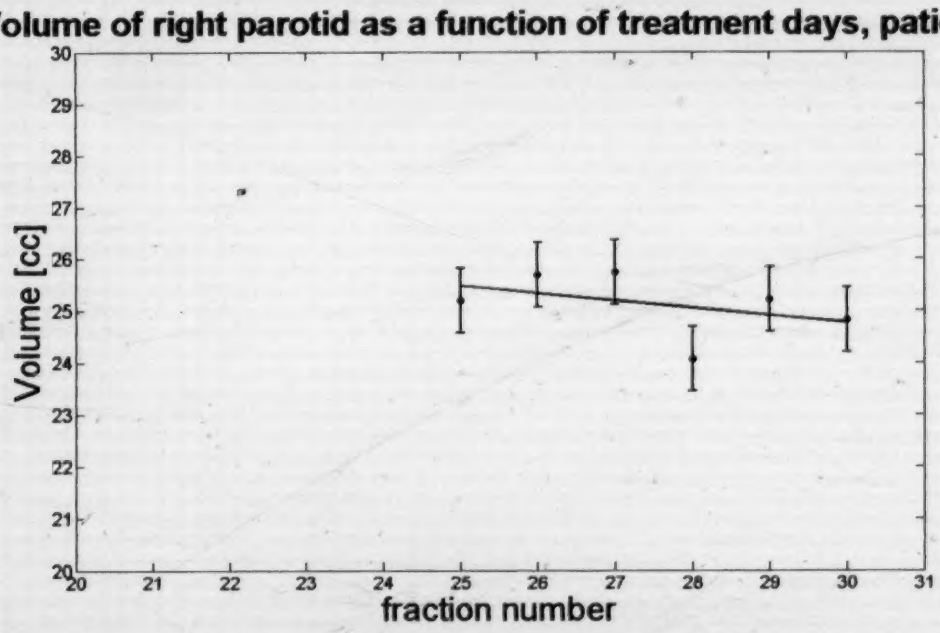

Figure 3-8. Linear regression results of the volume of right parotid for Patient 2

The data analysis of *Patient 3* reveals that the PTV60 values among chosen fractions are constant with the exception of 2 cases / data points (Table 3-4, Figure 3-9 –

3-12). In this patient, the PTV60 is located in deep within the head and neck anatomy and the patient outline almost never overlaps with the PTV60 – therefore the value of PTV60 volume appears to be constant. The contour of the PTV54 is located in close proximity to the superficial skin layers and the shrinkage overlaps with the area of the PTV54 in some slices. As a consequence, a volume change is observed and the PTV54 values vary among fractions. Linear regression gives the slope equal to -1 cc/fraction and this value is slightly greater than two standard deviation values away from zero.

Furthermore, analysis of the data shows that the slope of the right parotid is equal to 0.018 cc/fraction, whereas for the left parotid it nearly zero (volumes statistically stable).The average total percentage loss of the initial volume is equal 0.04% for the left and 0.4% for the right parotid. Overall, the patient is eligible for dose recalculation for chosen fractions and his anatomy can be assumed to be stable.

Patient 3				
	PTV60	PTV54	Left parotid	Right parotid
initial volume (cc)	112.1800	918.1	20.04	19.36
Slope (cc / fx)	0.0007	-1.0	0.003	0.018
slope error (cc / fx)	0.0005	0.4	0.002	0.009
Intercept (cc)	112.16	920	19.97	18.9
intercept error (cc)	0.01	11	0.05	0.2
R^2	0.1	0.3	0.1	0.3

Table 3-4. Linear regression results of VOIs for Patient 3

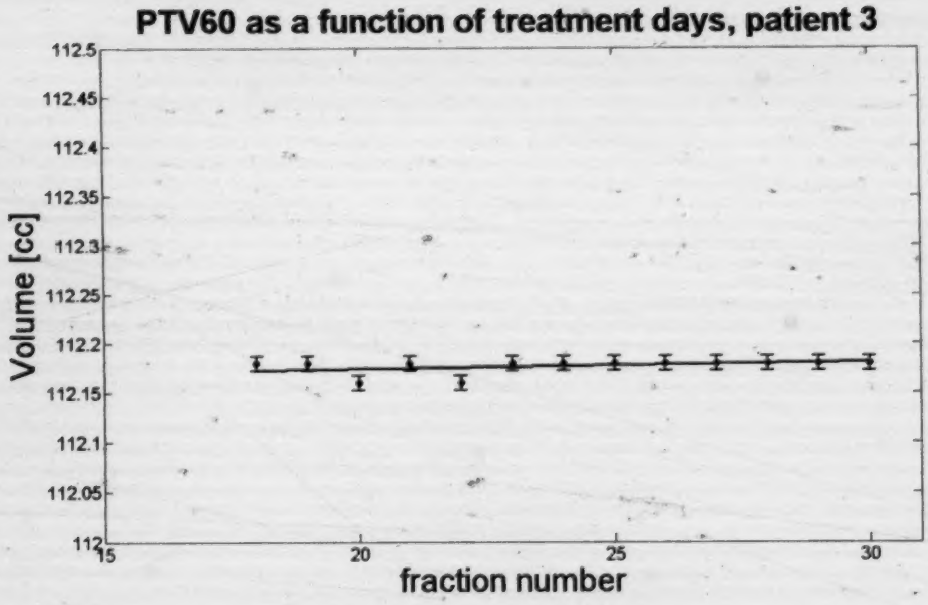

Figure 3-9. Linear regression results of the PTV60 for Patient 3

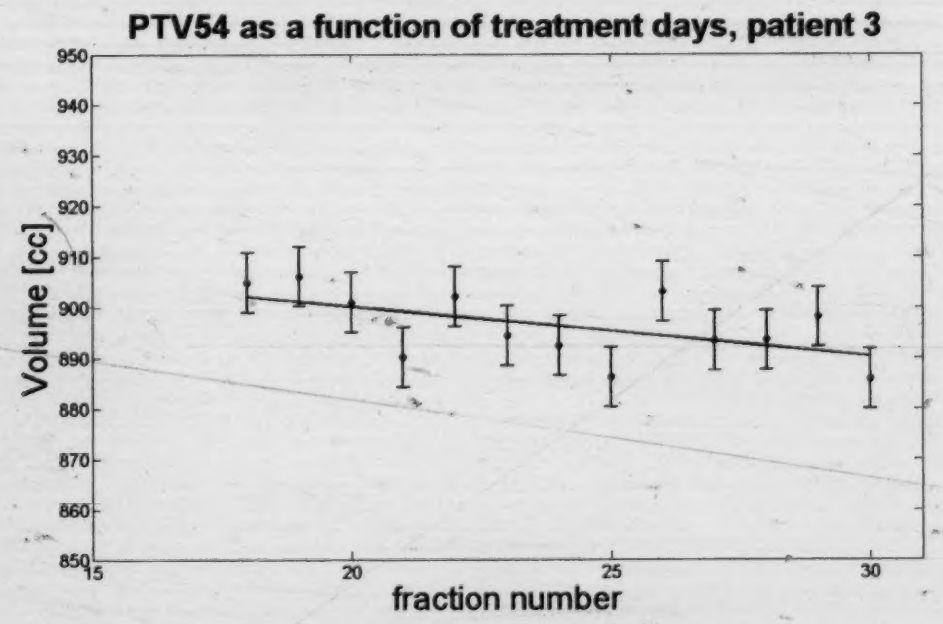

Figure 3-10. Linear regression results of the PTV54 for Patient 3

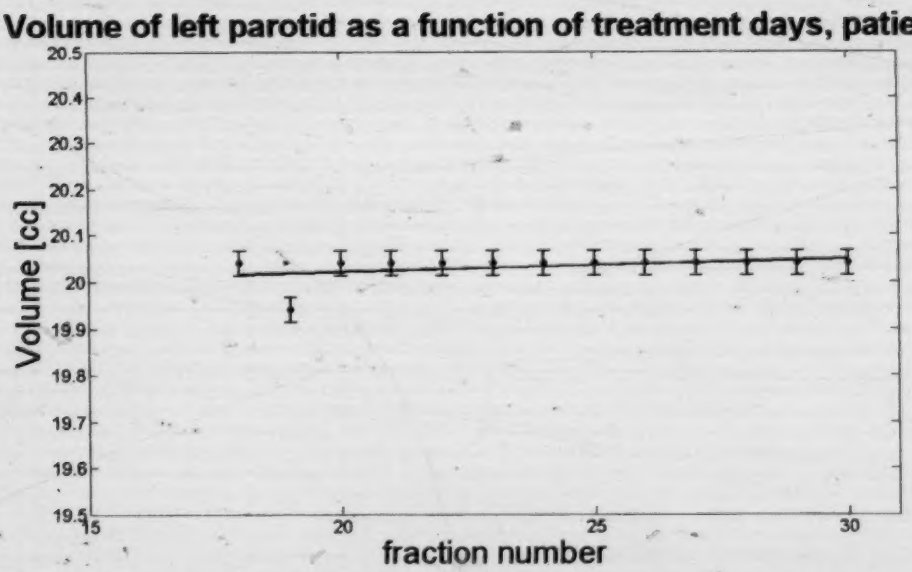

Figure 3-11. Linear regression results of the volume of left parotid for Patient 3

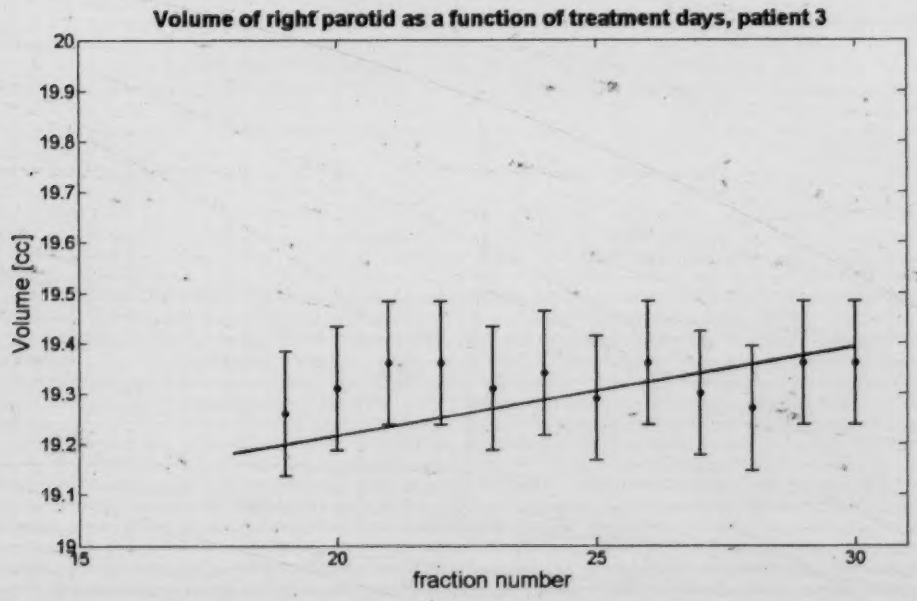

Figure 3-12. Linear regression results of the volume of right parotid for Patient 3

Patient 4 experienced significant weight loss/shrinkage and 10 fractions were deemed to be stable in terms of patient anatomy (Table 3-5, Figure 3-13 – 3-16). Since the PTV60 and PTV54 are both located near superficial layers of the head and neck

anatomy, the changes of their volumes are significant. The volume readings differ greatly for the PTV54 resulting in a slope of 4.5 cc/fraction (volume statistically unstable). For the PTV60, the slope is -0.84 cc/fraction (volume statistically stable). The best fit lines for the parotids in *Patient 4* have non-zero slopes and the values are equal to -0.36 cc/fraction for the left and -0.35cc/fraction for the right parotid. Both values are slightly greater than two error values. Also, the total average percentage loss of the initial volume is equal to 16.4% for the left and 10.5% for the right parotid.

Patient 4				
	PTV60	PTV54	Left parotid	Right parotid
initial volume (cc)	148.9	1285.1	28.4	27.3
slope (cc / fx)	-0.8	-4.4	-0.4	-0.4
slope error (cc / fx)	0.7	1.9	0.2	0.1
intercept (cc)	151	1308	33	33
intercept error (cc)	19	49	4	4
R^2	0.1	0.4	0.4	0.5

Table 3-5. Linear regression results of VOIs for Patient 4

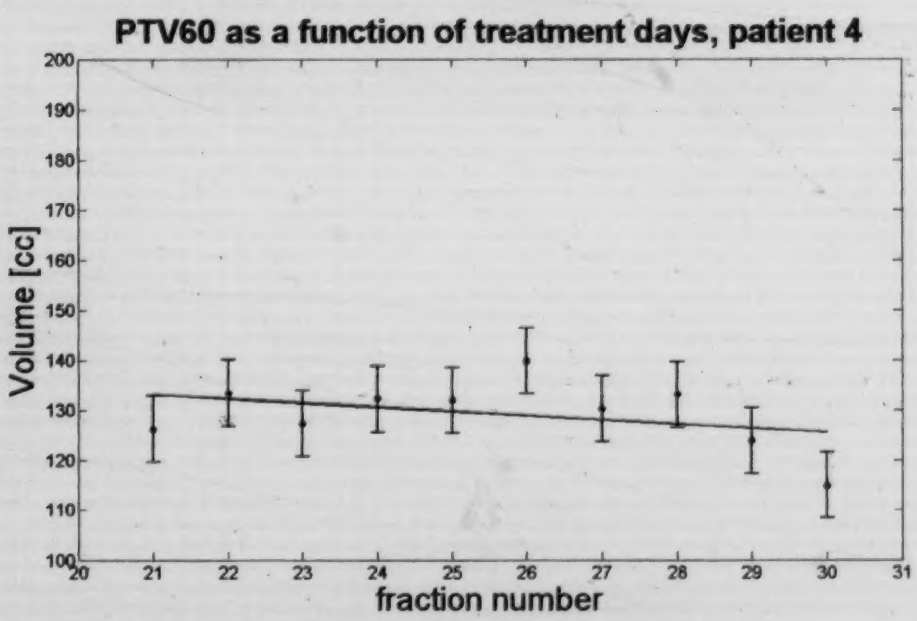

Figure 3-13. Linear regression results of the PTV60 for Patient 4

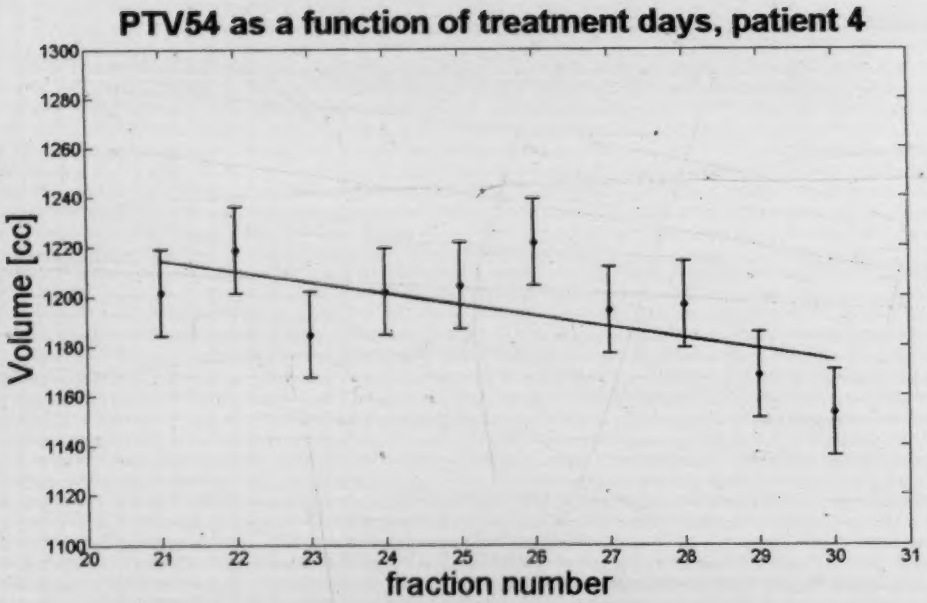

Figure 3-14. Linear regression results of the PTV54 for Patient 4

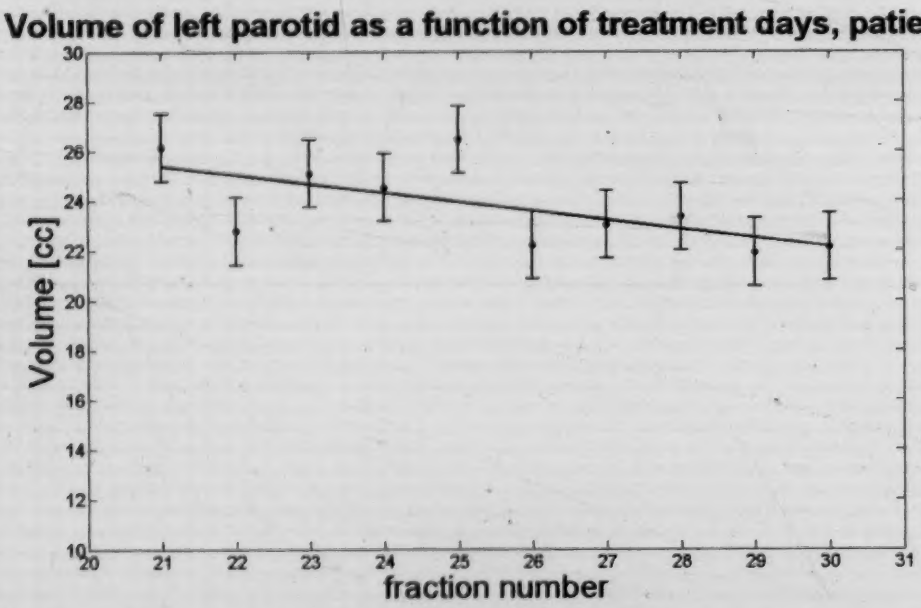

Figure 3-15. Linear regression results of the volume of left parotid for Patient 4

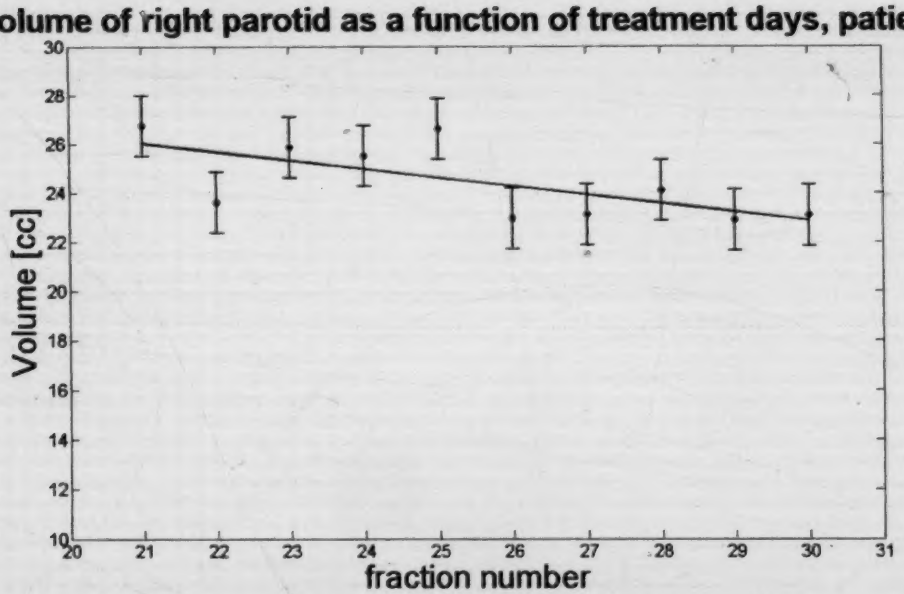

Figure 3-16. Linear regression results of the volume of right parotid for Patient 4

In the case of *Patient 5,* shrinkage is also apparent. Stabilization of the anatomy is seen over the last 11 fractions according to the preliminary assessment (Table 3-6, Figure 3-17 - 3-20). Both PTVs experience significant volume changes since they are located near the superficial layers of the patient's outline. The PTV60 slope for Patient 5 is the largest among PTV60 slopes for all patients and is equal to -1.3 cc/fraction. Similarly, the slope of the PTV54 best fit lines is also larger than for all other patients with a value of -5.9 cc/fraction. Linear regression performed for the parotid glands gives a positive slope of 0.7 cc/fraction for the left parotid (volume statistically stable and the greatest parotid slope for all patients) and a small negative slope of 0.1 cc/fraction for the right parotid (volume statistically stable). In addition, the left parotid lost on average 15.5% of its initial volume. The total volume loss in right parotid was 14.2%.

Patient 5				
	PTV60	PTV54	Left parotid	Right parotid
initial volume (cc)	304.5	1528.4	34.0	31.8
Slope (cc / fx)	-1.3	-5.9	0.7	-0.1
slope error (cc / fx)	0.4	2.7	0.2	0.2
intercept (cc)	331	1593	12	30
intercept error (cc)	9	67	5	5
R^2	0.6	0.4	0.6	0.02

Table 3-6. Linear regression results of VOIs for Patient 5

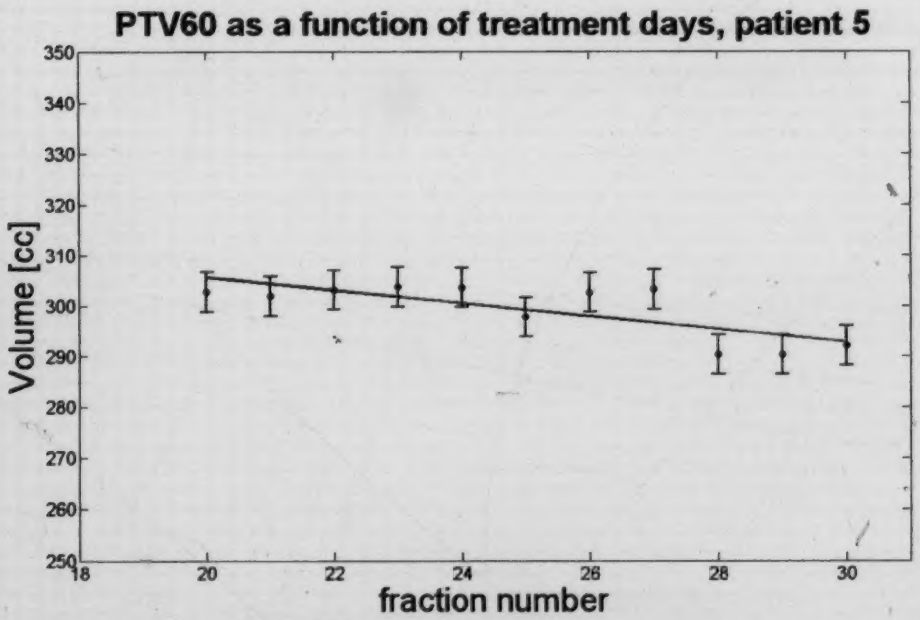

Figure 3-17. Linear regression results of the PTV60 for Patient 5

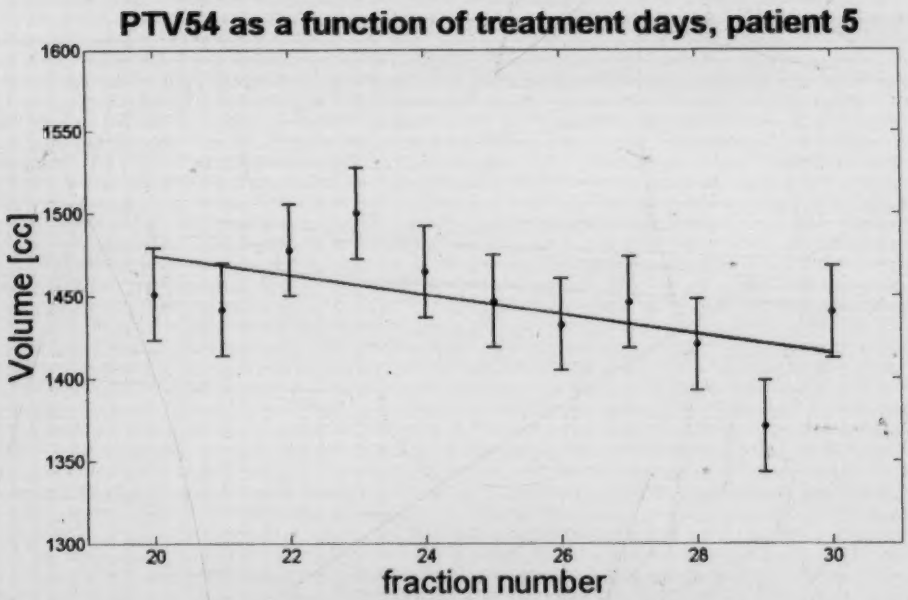

Figure 3-18. Linear regression results of the PTV54 for Patient 5

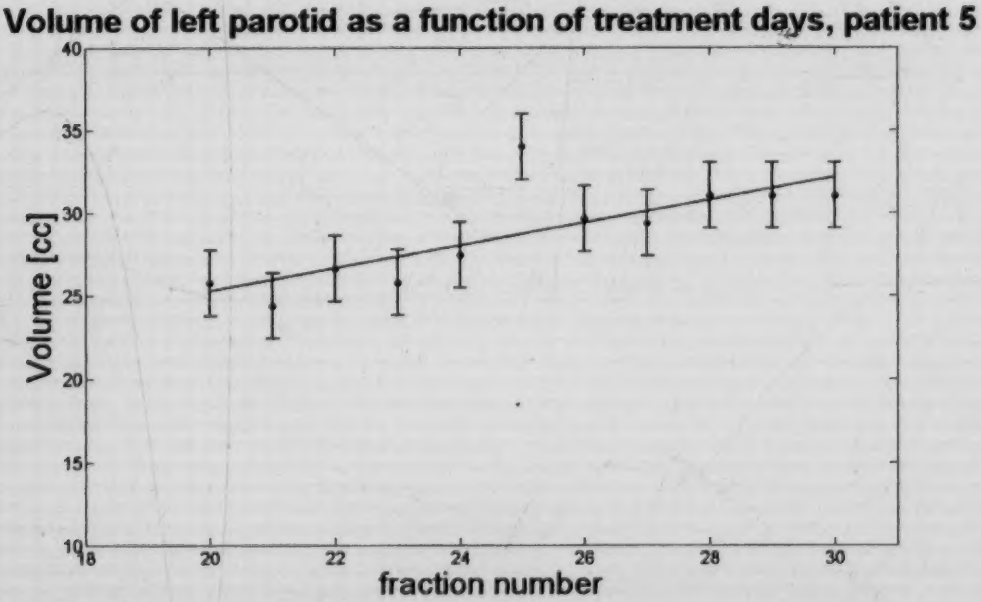

Figure 3-19. Linear regression results of the volume of left parotid for Patient 5

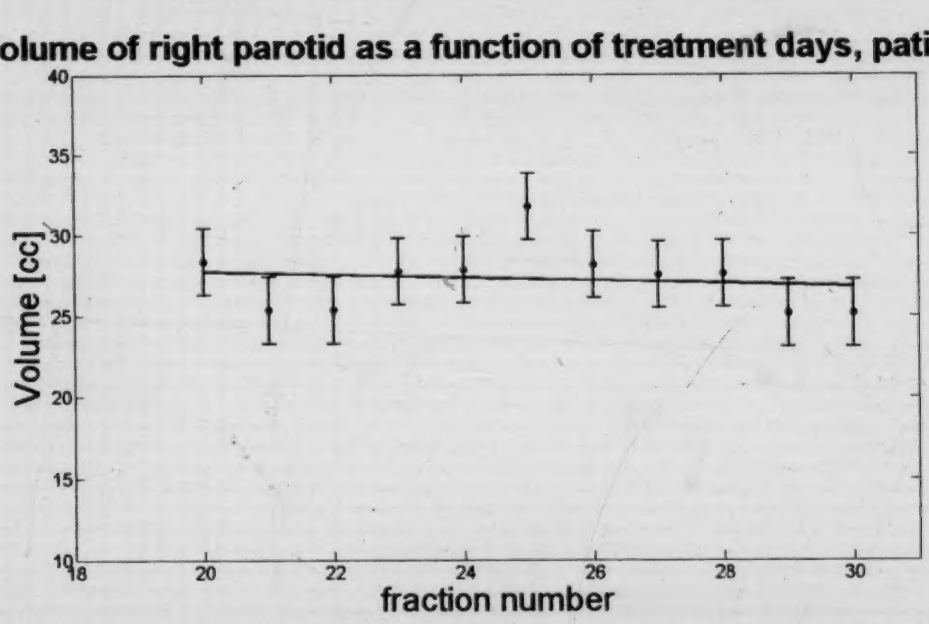

Figure 3-20. Linear regression results of the volume of right parotid for Patient 5

The analysis of the percentage change per fraction of a volume that is assumed to be stable with respect to its initial volume gives additional information about the degree of volume change (Table 3-7). In general, the changes in the PTV54 among fractions that are assumed to be stable in all treated patients are not greater than 0.4% of the initial volume per fraction - this is considered negligible. A similar situation is observed for the PTV60 where the maximum percentage loss of the volume among fractions that are assumed to be stable is not greater than 0.5%. The cord volume and the volume of the cord + 0.5 cm margin both remain constant, which is not surprising, as most of the perceived changes are related to outline variations. In addition, the spinal cord is surrounded by bony anatomy therefore the volume changes would not be observed even if re-contoured images have better soft tissue contrast. Of all the VOIs considered, the parotid volumes show the greatest variation. In some cases a volume gain is detected. The greatest differences are observed in *Patient 5* where the change is 2% of the initial planning volume per fraction in left parotid (volume gain) and in *Patient 4* where the volume change is 1.4% of the initial volume per fraction for left and 1.5% for the right parotid (volume loss in both parotids). In the left parotid of Patient 2, a 0.9% change of

the volume per fraction with respect to initial volume is seen among fractions that are assumed to be stable.

Patient no.		PTV60	PTV54	Left parotid	Right parotid
1	initial volume (cc)	499.1	904.6	16.36	21.76
	Slope (cc / fx)	-0.6	-0.6	0.04	-0.02
	% vol. change per fraction	***-0.1***	***-0.1***	***0.24***	***-0.09***
2	initial volume (cc)	181.77	1160.4	21.7	26.1
	Slope (cc / fx)	0.09	-2.2	0.2	-0.1
	% vol. change per fraction	***0.05***	***-0.2***	***0.9***	***-0.4***
3	initial volume (cc)	112.1800	918.1	20.04	19.36
	Slope (cc / fx)	0.0007	-1.0	0.003	0.02
	% vol. change per fraction	***0.0006***	***-0.1***	***0.015***	***0.09***
4	initial volume (cc)	148.9	1285.1	28.4	27.3
	Slope (cc / fx)	-0.8	-4.4	-0.4	-0.4
	% vol. change per fraction	***-0.5***	***-0.3***	***-1.4***	***-1.5***
5	initial volume (cc)	304.5	1528.4	34.0	31.8
	Slope (cc / fx)	-1.3	-5.9	0.7	-0.1
	% vol. change per fraction	***-0.4***	***-0.4***	***2.1***	***-0.3***

Table 3-7. Percentage volume changes per fraction for all patients.

3.2. Dosimetric analysis

Dosimetric analysis of the *Patient 1* dataset revealed that the summed dose is always higher than the planned dose (Table 3-8) for all given OAR constraint points defined by the in-house head and neck treatment protocol. The planned dose for the left parotid did not meet the gland sparing requirements – it should be noted that 57.1 Gy was planned to be delivered to this gland; due to its proximity to the PTV60, it was not possible to spare the left parotid. As a consequence, the delivered dose to the left parotid exceeds the maximal allowable dose, but the dose was only 0.6% higher than planned. The location of the tumour in the proximity of the parotid gland is responsible for the fact that the ROI is overdosed in this particular patient. Half (50%) of the right parotid volume obtained a significantly higher dose (7.8% greater than planned) therefore the gland sparing is not as good as was planned. The cord and cord plus 0.5 cm margins also

received higher doses than planned – the differences were found to be respectively equal to 7.3% and 6.3%.

In the case of the PTVs, the dose delivered is slightly greater but no hotspots are created. The PTV60 does not obtain a significantly higher dose and the maximal dose is 2.2% greater.

% dose difference, Patient 1					
	20% volume	50% volume	90% volume	99% volume	Max dose
PTV60	**2.2**	[illegible]	**1.5**	**1.2**	*2.2*
PTV54	[illegible]	[illegible]	**1.0**	[illegible]	*2.5*
Right parotid	[illegible]	**7.8**	[illegible]	[illegible]	*4.2*
Left parotid	[illegible]	**0.6**	[illegible]	[illegible]	*2.8*
cord+0.5 cm	[illegible]	**6.3**	[illegible]	[illegible]	*1.8*
cord	[illegible]	**7.3**	[illegible]	[illegible]	*4.4*

Table 3-8. Percentage dose difference between delivered and planned treatment for Patient 1 (sparing failure highlighted in red; note: in this case treatment plan was failing to satisfy the dose constraint for the left parotid).

The dose delivery analysis for *Patient 2* shows that the target volumes as well as OARs, in general, received higher dose at the constraint points than predicted. The exceptions to this were the cord and cord plus 0.5 cm where the dose is smaller by 2.5% and 0.8% respectively. On the other hand, the maximal dose to the cord increases by 4.9%. The dose delivery to the parotids exceeded the dose threshold constraint indicated in the protocol. In addition, the dose difference for the left parotid was found to be substantial at 25.7%; for the right parotid it is 2.7%. Furthermore, 90% of the PTV60 receives a dose that is 2.1% higher than planned, 50% of the volume receives 2.8% higher than planned and 20% of the volume receives 3% more than planned. The maximal dose is delivered to nearly the same volume as planned (0.1% difference). The PTV54 received maximal dose greater by 3.1%. Generally, the PTV54 does not receive a dose significantly different than the planned dose.

% dose difference, Patient 2					
	20% volume	50% volume	90% volume	99% volume	Max dose
PTV60	**3.0**	2.8	**2.1**	**1.7**	*0.1*
PTV54	2.1	0.0	**-0.4**	1.4	*3.1*
Right parotid	0.9	**2.7**	1.6	0.0	*2.2*
Left parotid	9.3	**25.7**	1.4	0.9	*3.2*
cord+0.5 cm	0.7	**-2.5**	0.0	-7.7	*4.9*
cord	0.6	**-0.8**	1.4	0.0	*1.8*

Table 3-9. Percentage dose difference between delivered and planned treatment for Patient 2 (sparing failure highlighted in red).

The dose delivery to *Patient 3* is as follows: delivered doses to the PTV60 are similar to planned doses – delivered doses are less than 2% higher for given % volumes defined by the protocol constraints. In contrast, the median dose to the right parotid volume is greater by 10.8%; however, the protocol dose constraint is still satisfied. Since the main tumour mass is located on the right side of the head and neck anatomy, noticeable shrinkage on the right side may explain the overdosage (gland displacement and volume loss are observed).

The left parotid accurately received the planned dose to 50% of its volume. In the case of the cord, the dose delivered is found to be 4.8% greater than predicted but delivery does not lead to failure of the cord sparing constraint as the maximum dose is still below 45 Gy. The maximal dose is also higher; the difference is calculated to be 4%. The cord with margin receives 7.3% higher maximal dose than predicted. Finally, 50% of the mentioned OAR receives 2.5% higher dose than planned.

% dose difference, Patient 3					
	20% volume	50% volume	90% volume	99% volume	Max dose
PTV60	**1.5**	0.7	**0.1**	**0.0**	*1.9*
PTV54	0.7	0.2	**1.5**	7.1	*0.3*
Right parotid	18.0	**10.8**	-1.2	-0.4	*1.3*
Left parotid	0.0	**0.0**	2.6	-4.6	*0.0*
cord+0.5 cm	0.9	**2.5**	0.5	-2.4	*7.3*
cord	0.8	**4.8**	0.8	-1.0	*4.0*

Table 3-10. Percentage dose difference between delivered and planned treatment for Patient 3.

The PTV60 of Patient 4 receives a dose that agrees with the planned dose to within 2% accuracy. The only significant difference is found in maximal dose – the delivered dose is greater than the planned dose by 35.6%. Since the main tumour mass is located on the left side and *Patient 4* experiences great shrinkage/weight loss, extensive overdosage of the left parotid is observed and the difference from the intended dose is 86.7% greater than planned. This leads to sparing failure in terms of the dose constraints. Conversely, sparing of the right parotid is better since the dose delivered is 1.5% smaller than predicted. The cord and the cord plus 0.5cm margin are also better spared and the differences between planned and delivered doses are respectively equal to -0.5% and -0.8%. However, the maximal doses to the cord / cord + 0.5 cm increased by 3 % and 7 % respectively.

% dose difference, Patient 4					
	20% volume	50% volume	90% volume	99% volume	Max dose
PTV60	**1.6**	1.2	**-0.4**	**-1.2**	*35.6*
PTV54	0.4	-0.2	**-1.1**	-1.7	*1.1*
Right parotid	7.2	**-1.5**	-0.2	0.5	*-0.3*
Left parotid	34.2	**86.7**	15.6	11.4	*2.5*
cord+0.5 cm	0.9	**-0.5**	-1.7	-2.5	*3.0*
cord	1.0	**-0.8**	-2.3	-2.1	*7.0*

Table 3-11. Percentage dose difference between delivered and planned treatment for Patient 4 (sparing failure highlighted in red).

Dosimetric analysis for *Patient 5* reveals that the PTV60 receives higher doses than predicted by, on average, 1.9 %. The maximal dose is 4.2% higher. Similarly, the dose delivered to the PTV54 is not significantly higher and does not exceed 2% for all of the constraint points defined in the protocol. In addition, the maximal dose is higher by 3.5%. Even though the tumour is located at the front of the head and neck anatomy, the difference in the accuracy of plan delivery for the parotids is not similar. The left parotid is significantly overdosed (30.6%) and this leads to failure in the sparing of this organ, according to the protocol constraints. The right parotid gland obtains a dose that is 3% smaller than predicted. The cord appears to have worse sparing than planned since the maximal dose increases by 7%. The same trend is noticed with cord plus 0.5cm where the maximal dose is greater by 8.3%.

% dose difference, Patient 5					
	20% volume	50% volume	90% volume	99% volume	Max dose
PTV60	**3.1**	[illegible]	**2.2**	**1.6**	*4.2*
PTV54	[illegible]	[illegible]	**0.6**	[illegible]	*3.5*
Right parotid	[illegible]	**-3.0**	[illegible]	[illegible]	*-2.7*
Left parotid	[illegible]	**30.6**	[illegible]	[illegible]	*3.5*
cord+0.5 cm	[illegible]	**-0.2**	[illegible]	[illegible]	*7.0*
cord	[illegible]	**-0.8**	[illegible]	[illegible]	*8.3*

Table 3-12. Percentage dose difference between delivered and planned treatment for Patient 5.

4. Discussion

There are several sources of uncertainty that may affect the results obtained in the study. They are related to the limitations of the method such as software capabilities, method and user dependent variables. The main limitation concerns the fact that stable patient anatomy has to be assumed due to the fact that the software is only capable of rigid body registration and non-deformable dose summation. Stable anatomy in head and neck cancers is an assumption that is not often possible to make because a significant number of patients lose weight gradually over the ***entire*** course of treatment [Bajaj et al., 2006, Barker et al., 2004, Senkus-Konefka et al., 2006]. This effect is often associated with a shift of the parotid glands into higher dose regions and with loss of parotid volume. Even among patients for whom the shrinkage in the patient outline appears to be absent, some volume changes in the ROIs are still observed. However, those volume changes may be related to the accuracy of contouring tools available in the *Planned Adaptive* software. The choosing of the patients who appeared to have stabilized, and which of the fractions that are assumed to be stable, was made by length measurement, as previously described, and its accuracy is dependent on the image resolution in the chosen plane. Furthermore, the tools offered for re-contouring purposes are very basic and new margins of given VOIs have to be drawn manually on each slice for each fraction. In addition, re-contouring is performed on lower resolution merged kVCT-MVCT images which have poor soft tissue contrast for contour delineation in comparison to the resolution and contrast of treatment planning image. PTVs is more difficult to re-contour

accurately due to the lack of visibility or absence, in post surgery patients, of the GTV on those images. As a consequence, PTVs are adjusted to the patient outline only. Thus, volume readings are just an approximation of the real size of PTV and therefore volume changes can be only roughly evaluated. Consequently, PTV volume readings are dependent on the level of shrinkage/weight loss; however, it is observed that they should also rely on the position of the GTV, if present.

Additional uncertainty in the PTV volume changes analysis is related to the variable number of MVCT slices for different fractions but this concerns the analysis done for *Patient 1* only. It is observed that the volume changes are strongly related to the number of MVCT slices available for a given fraction. Because of the fact that this one patient experienced extensive shrinkage with respect to the pre-treatment anatomy and the PTVs are large (PTV54 extended over 51 slices and PTV 60 extended over 43 slices), the variable MVCT coverage of PTV (21 slices for PTV54 or to 16 slices for PTV60) introduced uncertainty to those data. In addition, it was readily apparent that the extensive shrinkage enabled greater mobility of the patient within the mask which also added the uncertainty to the volume readings as re-contouring was done with respect to patient outline.

In other cases the MVCT coverage is complete in the areas of PTV where shrinkage occurs with exception to one single fraction for Patient 5.

Due to the low contrast resolution of the images, the parotid gland outline is not easily visible; therefore, re-contouring is guided by the original contours, the position of the mandible and a distance assessment from the patient outline. Also, since parotids are small in volume, slight inaccuracies in re-contouring result in large relative errors in the volume reading.

Since shrinkage results in a certain level of mobility of the head and neck anatomy within the immobilization mask, anatomical rotations are present and different setup shifts for different regions of anatomy are observed. This may also add some uncertainty to the contoured ROIs and, as a consequence, to volume readings.

It is expected that towards the end of the treatment (over the last fractions that are assumed to be stable), any changes in VOI values will show a decreasing trend [Bajaj et al., 2006, Barker et al., 2004, Senkus-Konefka et al., 2006]. Positive slopes and statistical

instability are believed to arise most likely from the limitations of the method, from observer variability, or from the small sample of data points.

The dataset of volume changes relative to the initial / planning volume of given ROI is also influenced by the factors noted previously. The volume changes are negligible for *Patient 3* and the greatest change among all VOIs is equal to 0.1% per fraction (PTV54). Similarly, the analysis of *Patient 1* shows satisfactory results and this patient is therefore certainly eligible for dose delivery assessment.

In general, the changes in PTV volumes among analyzed fractions are small in all patients with respect to corresponding initial volume. They do not exceed 0.6% per fraction.

Patients 4 & 5 have the greatest volume changes for all ROIs considered. The parotid glands in each patient (except for right parotid in *Patient 5*) change by more than 1.2 % per fraction (max 2,0% per fraction). Therefore, according to this part of the analysis these patients seem to show anatomical instability; however, dosimetric analysis is still performed for them since the data includes a considerable level of uncertainty. As such, the final dosimetric results must be treated with caution.

The volume changes for the parotid glands of *Patient 2* are statistically insignificant. In addition, the left parotid changes by approximately 1% from fraction to fraction. This, however, is a positive increment and as stated before it is not likely to reflect reality. *Patient 2* is nevertheless assumed to be appropriate for dose delivery assessment.

In general, the dosimetric analysis reveals that the dose delivered to selected VOIs to the patients that experienced initial shrinkage (but stabilized later in the course of treatment, i.e. for the analyzed fractions) is usually greater than predicted by the plan. The dose received by target volumes is not significantly different though - dose inhomogeneity and the possible creation of hotspots and cold spots is a greater concern. In the case of organs at risk, the dose delivered is often greater and leads to sparing failure in some cases - especially in parotids. This is the main reason why treatments should be adapted to the changing anatomy with the currently available technique. The displacement of anatomy and volume loss in the patient is largely responsible for failure to achieve treatment objectives. In addition, immobilization seems to be less effective due

to shrinkage/weight loss and influences the treatment delivery in general. The differences in the dose given to the cord and the cord plus 5mm margin is also caused by rotation of the anatomy that are observed in the images and variable setup shifts in different parts of the head and neck anatomy. The limitations of the software also introduce some errors in the results; for example, the variability in manual re-contouring, given the low contrast in the images and as well as inter-user variability in contouring, impacts the volumetric part of the study as mentioned previously. However, because the volumetric part of the analysis is strongly related to the dosimetric part (since the contours define the ROIs and allow creation of DVHs), the errors in contouring influence the interpretation of the dosimetric results. Also, only one set of the contours for one fraction is used for the calculation of DVHs from the summation doses. In the case of the cord, even though its volume does not change, the variable shift among analyzed fractions can cause an alteration of the dose especially in the situation where the immobilization mask is not well adjusted to the neck area.

The results of the study indicate that some of the H&N patients will likely benefit from the incorporation of adaptive treatment. It is observed that the greatest changes with respect to the initial patient anatomy are present during the second half of the course of treatment. Therefore, if the introduction of a single adaptive plan into the treatment is considered, it should be done for the second half of the treatment fractions. This is not only apparent from our data, but is also supported by the literature [Barker et al]. Adaptation of the treatment plan can also enhance OAR sparing, target coverage and dose homogeneity.

Unfortunately due to software limitations such as rigid body image registration and non-deformable dose summation, dose delivery assessment cannot be done for all patients. However, the study indicates that adaptive planning would certainly improve dose distribution in cases where such distributions are not acceptable.

5. Conclusions

H&N patients often experience shrinkage/weight loss during the course of treatment. A stabilization of the anatomy is achieved in some cases (i.e. no more

shrinkage occurs beyond a certain point in the course of treatment). A very precise assessment of volumetric changes is not, however, possible with the currently available HT *Planned Adaptive* software. The shrinkage in the patient causes displacement of the parotid glands as well as poorer immobilization of head and neck anatomy (due to more loosely fitting immobilization mask) consequently results in a deterioration of the positioning accuracy. Due to those reasons, the overdosage of the OARs and an increase in inhomogeneity within the target volumes may be present. The software enables dose delivery assessment; however, if the calculated results are expected to be close to the reality, the assessment must currently be performed only for patients that have stable or stabilized anatomy. Changes in anatomy and its dosimetric consequences in some patients suggest adaptive planning at some point in the treatment course, if our aim is to maintain OAR sparing.

Bibliography

Bajaj GK, Teslow T, Yu MH, Lee DJ, Ford DJ. "Megavoltage CT assessment of volume changes in target and non-target tissues of the head and neck over a standard course of therapy" *Int J Radiat Oncol Biol Phys* 66(3), Supplement (2006).

Barker JL, Garden AS, Ang KK, O'Daniel J, Wang H, Court LE, Morrison WH, Rosenthal DI, Chao C, Tucker SL, Mohan R, Dong L. "Quantification of volumetric and geometic changes occurring during fractionated radiotherapy for head-and-neck cancer using an integrated CT/linear accelerator system" *Int J Radiat Oncol Biol Phys* 59(4):960–970 (2004).

Barkley HT, Fletcher GH. "The significance of residual disease after external irradiation of squamous-cell carcinoma of the oropharynx" *Radiology* 124:493–495 (1977).

Butler EB, Teh BS, Grant WH, Uhl BM, Kuppersmith RB, Chiu JK, Donovan DT, Woo SY. "SMART (Simultaneous Modulated Accelerated Radiation Therapy) Boost: A new accelerated fractionation schedule for the treatment of head and neck cancer with intensity modulated radiotherapy" *Int J Radiat Oncol Biol Phys* 45(1):21-32 (1999).

Eisbruch A, Haken RKT, Kim HM, Marsch LH, Ship JA. "Dose, volume, and function relationships in parotid salivary glands following conformal and intensity modulated irradiation of head and neck cancer" *Int J Radiat Oncol Biol Phys* 45(3):577–587 (1999).

Hansen EK, Bucci MK, Quivey JM, Weinberg V, Xia P. "Repeat CT imaging and replanning during the course of IMRT for head-and-neck cancer "*Int J Radiat Oncol Biol Phys* 64(2):355–362 (2006).

Li Y, Taylor JMG, Haken RKT, Eisbruch A."Impact of dose on parotid salivary recovery in head and neck cancer patients treated with radiation therapy" *Int J Radiat Oncol Biol Phys* 67(3):660–669 (2007).

Miszczyk L, Wydmanski J. "Evaluation of Delivered Dose Changes During Radiation Therapy" *Acta Oncologica* 38(2):197–201 (1999).

Munter MW, Hoffner S, Hof H, Herfarth KK, Haberkorn U, Rudat V, Huber P, Debus J, Karger CP."Changes in Salivary Gland Function After radiotherapy of head and neck tumours measured by quantitaive pertechnetate scintigraphy: Comparison of intensity modulated radiotherapy and conventional radiation therapy with and without amifostine" *Int J Radiat Oncol Biol Phys* 67(3):651–659 (2007).

Roesink JM, Moerland MA, Battermann, JJ, Hordjik GJ, Terhaard CHJ. "Quantitative dose-volume response analysis of changes in parotid gland function after radiotherapy in the head-and-neck region" *Int J Radiat Oncol Biol Phys* 51(4):938–946 (2001).

Scrimger R, Stavrev P, Parliament MB, Field GC, Thompson H, Stavreva N, Fallone BG. "Phenomenologic Model Describing Flow Reduction for Parotid Gland Irradiation with Intensity-Modulated Radiotherapy: Evidence of Significant Recovery Effect", *Int J Radiat Oncol Biol Phys* 60(1):178-185 (2004).

Senkus-Konefka E, Naczk E, Borowska I, Badzio A, Jassem J. "Changes in lateral dimensions of irradiated volume and their impact on the accuracy of dose delivery during radiotherapy for head and neck cancer" *Radiotherapy and Oncology* xx:1–6 (2006) *in press.*

Sobel S, Rubin P, Keller B, *et al.* Tumor persistence as a predictor of outcome after radiation therapy of head and neck cancers. *Int J Radiat Oncol Biol Phys* 1:873–880 (1976).

Suit HD, Walker AM. "Assessment of the response of tumours to radiation: Clinical and experimental studies". *Br Cancer Suppl* 41:1–10 (1980).

Warkentin B, Stavrev P, Stavreva N, Field C, Fallone BG. "A TCP-NTCP estimation module using DVHs and known radiobiological models and parameter sets". *J Appl Clin Med Phys* 5:50–63 (2004).

Yamashita H, Nakagawa K, Nakamura N, Abetakahiro K, Ohmoto A, Okada S, Matsumoto I, Hosoinakashi, Sasano YH, Yamakawa S, Ohtomo K. "Relation between acute and late irradiation impairment of four basic tastes and irradiated tongue volume in patients with head ad neck cancer" *Int J Radiat Oncol Biol Phys* 66(5):1422–1429 (2006).

Zhang L, Garden AS, Lo J, Ang K, Ahmad A, Morrison WH, Rosenthal DI, Chambers MS, Zhu XR, Mohan R, Dong L. "Multiple regions-of-interest analysis of setup uncertainties for head-and-neck cancer radiotherapy" *Int J Radiat Oncol Biol Phys* 64(5):1559–1569 (2006).

Chapter 4. Summary

The work presented in this thesis is important from the perspective of conformal radiotherapy in general and HT in particular. Intrafraction motion is of great interest in radiation therapy and yet has not been thoroughly studied due to the limited availability of online volumetric image guidance. Therefore, Chapter 2 discusses the magnitude of intrafraction motion and is an important addition to the existing literature. Also, the study gives the reader some insight into the positioning accuracy for various sites, not limited to prostate, GBM and H&N sites as presented in this chapter. Furthermore a technique to revise the accuracy of currently used PTV margins is offered. For example, if the current PTV contour of a given site is found to be inadequate in comparison to the measured contour, the presented method may lead to a new PTV prescription.

The study showed that even patients with relatively modest immobilization (prostate, palliative treatment) have average translational shifts based on the post-treatment scan within 1 mm, and there were no large outliers noted (i.e. the medians of shifts are close to averages). Furthermore, data presented in Chapter 2 compared two different sites that are immobilized using exactly the same technique. In particular, it was found that the positioning accuracy in H&N was noticeably worse in comparison to GBM and the reason for that was likely weight loss and tumour shrinkage in H&N patients, resulting in a change in anatomy. Therefore it seems that in H&N cases, instead of PTV adjustment, adaptive treatment may be more effective.

In addition, Chapter 2 offers a technique that can be successfully used in-house based on the tools that are available on the HT unit. It should be underlined, that the presented data are meant to demonstrate how this technique would work and what sort of results and analysis one could apply. It is not meant to dictate to other institutions what appropriate margins are. Although the sample sizes are small, they are not out of line with related studies published recently [Millender et al., 2004; Murphy et al., 2003; Song et al., 2006]. This is especially true when one considers the spirit of the study, i.e. a proof in principle of a method that one can implement locally to use onboard imaging to evaluate, in house, the efficacy of immobilization and image guided setup. In addition, it is acknowledged that the sample may be too small to draw any meaningful universal

conclusions, but this is a demonstration of a useful technique. Furthermore, it should be also mentioned that there are papers published in the other journals presenting the studies that are designed based on small samples [Schaly et al., 2005; Song et al., 2005; Ullman et al., 2006].

Once a centre decides to use this technique, it should account for the time that is required for additional scanning (post treatment imaging) of the sites that are chosen for the positioning and PTV evaluation on a regular (most likely weekly) basis for the extended period of time, though the benefit of the additional treatment information is apparent.

Since the *Planned Adaptive* software became available soon after the first study described in Chapter 2, the dose delivery assessment for H&N sites experiencing anatomical changes was possible. However, due to the fact that the software is limited to rigid body registration and non-deformable dose summation, only selected patients whose anatomy changes had stabilized before the end of their treatment course could have their treatment delivery examined. The dose delivery assessment revealed that the greatest concern in H&N patients that experience anatomy changes is a deterioration in OAR sparing and in some cases failure to achieve the desired sparing. The overdosage of the parotid glands was due to shrinkage in patient, parotid volume loss and parotid displacement. The alteration in the dose delivered to the cord was caused by shrinkage in the patient, rotations and different shifts in various places of head and neck anatomy. However, the results obtained for each patient should be treated with some uncertainty due to limitations of the method that are more thoroughly described in Chapter 3.

Since the general observation made in the study are supported by the literature [Barker et al., 2004; Barkley et al., 1977; Butler et al., 1999; Eisenbruch et al., 1999; Hansen et al., 2006; Miszczyk et al., 1999; Senkus-Konefka et al., 2006; Sobel et al., 1976; Suit et al., 1980; Zhang et al., 2006] the utility of adaptive planning in selected H&N cases is evident and may be required to reduce median and maximum doses to selected tissues.

A general protocol for H&N adaptive radiotherapy should be developed, that takes into consideration time efficiency and maximal probability of dose delivery improvement. Therefore, it seems to be the most appropriate to implement adaptive

treatment before the start of the second half of the fractionation scheme (e.g. after 15 of 30 treatment fraction) based on the general trend of the anatomy changes in patients. The decision should also be based on daily dose delivery assessments, not on the summation of the daily doses, since for any given patient the summation dose is known to not give completely accurate results when changing volumes are involved. The adaptive planning software that is currently available can be used for the patients, however, with no shrinkage over last few fractions and it is only in this case that an accurate dose delivery assessment can be made. The current adaptive planning process, where it can be used with confidence, is very time inefficient. There is only one treatment planning station per HT unit in our centre and there is a heavy workload on it, and the time that is required for re-contouring makes it difficult to introduce the adaptive planning method in to the clinical setting. However, if it is decided to use the method more regularly, a standardization of the MVCT scanning technique for patients to be adaptively planned has to be introduced (i.e. an equal number of slices covering a consistent region, and at least the whole PTV, for each fraction). Once it is decided to re-plan at some point during the course of treatment, it seems to be most effective if the whole planning process is repeated for the remaining fractions. This would most likely require re-imaging with conventional kVCT scanner (CT-sim), and producing a new immobilization mask, as it has been seen that the weight loss experienced by H&N patients results in masks which no longer fit properly and it is assumed that this is the reason for the larger intrafraction variations noted in our study. In our centre, if the *Planned Adaptive* is used frequently it will be necessary to develop a new, faster DQA process. *TomoTherapy Inc.* is in the process of developing the enhanced version of *Planned Adaptive* software that is capable of non-rigid image registration and deformable dose summation. Once the upgrade of the software is commercially available and acquired by our centre, the adaptive process is expected to be more time efficient and applicable for all cases in terms of delivery assessment (the assumption of stable anatomy will be no longer required for dose delivery assessment). The re-contouring problem will not be quite of the same magnitude since the software will do an automatic re contouring, although these contours will be subject to review and possibly modification.

Further development of the research presented in this thesis should be performed. It is recommended that the follow up of the study presented in Chapter 3 be designed for a greater number of patients per site in order to obtain better statistics. Additionally, it is advised to invite additional people to take part in the contouring and/or treatment process, and to analyze data to discover any potential impact of inter-observer variability on the final results.

ART will certainly be an area of further intense research. In particular, adaptive planning on HT requires more investigation and with great certainty it can be said that the literature will be enriched with regard to these kinds of studies. It seems that as more advanced software becomes available (i.e. implementations of non-rigid image registration), more often the ART will be used in clinic.

Bibliography

Barker JL, Garden AS, Ang KK, O'Daniel J, Wang H, Court LE, Morrison WH, Rosenthal DI, Chao C, Tucker SL, Mohan R, Dong L. "Quantification of volumetric and geometic changes occurring during fractionated radiotherapy for head-and-neck cancer using an integrated CT/linear accelerator system" *Int J Radiat Oncol Biol Phys* 59(4):960–970 (2004).

Barkley HT, Fletcher GH. "The significance of residual disease after external irradiation of squamous-cell carcinoma of the oropharynx" *Radiology* 124:493–495 (1977).

Butler EB, Teh BS, Grant WH, Uhl BM, Kuppersmith RB, Chiu JK, Donovan DT, Woo SY. "SMART (Simultaneous Modulated Accelerated Radiation Therapy) Boost: A new accelerated fractionation schedule for the treatment of head and neck cancer with intensity modulated radiotherapy" *Int J Radiat Oncol Biol Phys* 45(1):21-32 (1999).

Eisbruch A, Haken RKT, Kim HM, Marsch LH, Ship JA. "Dose, volume, and function relationships in parotid salivary glands following conformal and intensity modulated irradiation of head and neck cancer" *Int J Radiat Oncol Biol Phys* 45(3):577–587 (1999).

Hansen EK, Bucci MK, Quivey JM, Weinberg V, Xia P. "Repeat CT imaging and replanning during the course of IMRT for head-and-neck cancer "*Int J Radiat Oncol Biol Phys* 64(2):355–362 (2006).

Millender LE, Aubin M, Pouliot J, Shinohara K, Roach M. "Daily electronic portal imaging for morbidly obese men undergoing radiotherapy for localized prostate cancer". *Int J Radiat Oncol Biol Phys* 59(1):6–10 (2004).

Miszczyk L, Wydmanski J. "Evaluation of Delivered Dose Changes During Radiation Therapy" *Acta Oncologica* 38(2):197–201 (1999).

Murphy MJ, Chang SD, Gibbs IC, Le Q, Hai J, Kim D, Martin DP, Adler JR. "Patterns of patient movement during frameless image-guided radiosurgery". *Int J Radiat Oncol Biol Phys* 55(5):1400–1408 (2003).

Schaly B, Bauman GS, Song W, Battista JJ, Van Dyk J. "Dosimetric impact of image-guided 3D conformal radiation therapy of prostate cancer" *Phys Med Biol 50(13) 3083-3101; (2005).*

Senkus-Konefka E, Naczk E, Borowska I, Badzio A, Jassem J. "Changes in lateral dimensions of irradiated volume and their impact on the accuracy of dose delivery during radiotherapy for head and neck cancer" *Radiotherapy and Oncology* 79(3):304–309 (2006).

Sobel S, Rubin P, Keller B, *et al.* Tumor persistence as a predictor of outcome after radiation therapy of head and neck cancers. *Int J Radiat Oncol Biol Phys* 1:873–880 (1976).

Song W, Schaly B, Bauman G, Battista J, Van Dyk J. "Image-guided adaptive radiation therapy (IGART): Radiobiological and dose escalation considerations for localized carcinoma of the prostate". *Med Phys* 32(7):2193-2203 (2005).

Song WY, Chiu B, Bauman GS, Lock M, Rodrigues G, Ash R, Lewis C, Fenster A, Battista JJ, Van Dyk J. "Prostate contouring uncertainty in megavoltage computed tomography images acquired with a helical tomotherapy unit during image-guided radiation therapy". *Int J Radiat Oncol Biol Phys* 65(2):595–607 (2006).

Suit HD, Walker AM. "Assessment of the response of tumours to radiation: Clinical and experimental studies". *Br Cancer Suppl* 41:1–10 (1980).

Ullman KL Ning H, Susil RC, Ayele A, Jocelyn L, Havelos J, Guion P, Xie H, Li G, Arora BC, Cannon A, Miller RW, Coleman CN, Camphausen K, Ménard C. "Intra- and

inter-radiation therapist reproducibility of daily isocenter verification using prostatic fiducial markers" *Radiation Oncology* 1:2 (2006).

Zhang L, Garden AS, Lo J, Ang K, Ahmad A, Morrison WH, Rosenthal DI, Chambers MS, Zhu XR, Mohan R, Dong L. "Multiple regions-of-interest analysis of setup uncertainties for head-and-neck cancer radiotherapy" *Int J Radiat Oncol Biol Phys* 64(5):1559–1569 (2006).